Electron transfer mechanistic manifold and variable transition state character. A theoretical investigation of model electron transfer processes between nucleophiles and ethane cation radical

A. Chandrasekhar Reddy, David Danovich, Alexander Ioffe and Sason Shaik *
Department of Organic Chemistry and the Fritz Haber Center of Molecular Dynamics, The Hebrew University, Jerusalem 91904, Israel

This paper addresses the question of an electron transfer mechanistic manifold by *ab initio* computations of the model systems $Nu: + C_2H_6^{\bullet+} \longrightarrow Nu^{\bullet+} + C_2H_6$ where, Nu ≡ H_2S, PH_3, H_2O and NH_3. The computations show that there exist two major classes of ET mechanisms. The first is *a concerted ET mechanism which proceeds along a maximum bonding trajectory.* The second class is a *stepwise ET mechanism which involves shuttles of redox pairs, e.g.*, $H^+/H^\bullet$ and $CH_3^+/CH_3^\bullet$, and thereby results in a single electron transfer from the nucleophile to the cation radical. Thus, an apparent ET may be a net result of consecutive steps which by themselves are non-ET steps. The genesis of the mechanistic manifold and variable transition state structure from valence bond (VB) configurations is discussed. It is found that all these mechanisms are typified by electronic structures that share the same set of VB configurations with variable proportions, giving rise thereby to variable transition state structure and an ET mechanistic family. The situation is reminiscent of the mechanistic manifold encountered in physical organic chemistry, *e.g.*, the S_N2 and S_N1 mechanisms in the classical nucleophilic substitution process. For all the $Nu:/C_2H_6^{\bullet+}$ combinations we also identified outer-sphere transition state analogues that avoid the bonding between the reactants. All the outer-sphere saddle points are found to be higher in energy than the bonded mechanisms of the concerted and stepwise varieties. It appears therefore, that *outer-sphere mechanisms should be regarded as default options rather than natural mechanisms of ET-reactions of cation radicals. Indeed, all the computational trends exhibited by the ET mechanistic manifold are shown to be the consequences of maximum bonding.*

A question that is still not entirely settled in organic electron transfer (ET)[1] chemistry, is: *how actually do two organic molecules transfer an electron between them?* There is an impressive body of evidence which indicates that ET reactions occur by direct pathways, *via* the weakly overlapping outer-sphere or inner-sphere transition states.[1,2] Nevertheless, alongside these concerted ET-mechanisms, there exist significant amounts of data on the occurrence of indirect or stepwise ET mechanisms; in which an *apparent* ET is a net result of consecutive steps which by themselves *are non-ET steps*, albeit possessing reactivity patterns resembling ET reactions.[1,3] This situation is reminiscent of the mechanistic manifold encountered in physical organic chemistry where many processes can occur *via* a family of related mechanisms, *e.g.*, the S_N2 and S_N1 mechanisms in the classical nucleophilic substitution process or the E1, E2 and $E1_{CB}$ mechanisms in the 1,2-elimination process.[4] Clearly, once this analogy applies to ET, it draws also the related analogy to the variable transition-state approach; in which the different mechanisms of a given process influence the transition state and endow it by a variable mixture of their own intrinsic characteristics, *e.g.*, an S_N2 transition state with variable S_N1 character, and so on. Does this analogy hold for ET? If so, could we find then a 'mechanistic spectrum' that allows us to conceptualize the structure of the ET transition state in terms of mixed character endowed by the potential stepwise mechanisms? If this turns out to be the case, then the entire culture of variable transition state approach[5] in physical organic chemistry would be brought to bear on mechanistic organic ET reactivity.†[6]

† Discussions of variable transition states in polar and ET reactions appeared in refs. 6(*a*), (*b*). A related discussion appeared in ref. 6(*c*), in terms of the extent of electron transfer in the transition state of a dissociative ET.

Nucleophile (Nu:)/cation radical ($RH^{\bullet+}$) combinations are known to undergo substitution processes,[7] proton transfer processes,[8] as well as electron transfer processes.[1] Moreover, our own recent computational studies,[9] have shown that the transition state for the model concerted-ET reaction of H_2S: and $C_2H_6^{\bullet+}$ possesses a robust stereochemistry and an unusual electronic structure. Therefore, the $Nu:/C_2H_6^{\bullet+}$ combinations appear at the outset as suitable target systems on which we may attempt to model the general question of the ET mechanistic manifold by *ab initio* computations. The specific model systems are shown in eqn. (1), where the double arrow implies the existence of stepwise ET as well as concerted ET mechanisms.

$$Nu: + C_2H_6^{\bullet+} \rightarrow\!\rightarrow Nu^{\bullet+} + C_2H_6; \quad Nu \equiv H_2S, H_2O, PH_3, NH_3 \quad (1)$$

The simplicity of the model systems is a source of strength as well as weakness. The weaknesses are obvious from a point of view of experimental feasibility. However, it is due to the simplicity of the systems that we are able to draw generalities concerning the topology of the potential energy profiles, as well as the electronic-structure variations associated with the various mechanisms discerned for eqn (1). The results provide for the first time a detailed comparison between the potential energy profiles of strongly bonded concerted and stepwise ET mechanisms with their weakly bonded outer-sphere options.

Theoretical methods and calculations

The various species were computed with the GAUSSIAN 92 and GAMESS 93 packages[10,11] using the 6-31G* basis set[12] at the UHF and UMP2 levels of theory. A few tests for consistency were also carried out at the ROHF and ROMP2 levels of theory. Mechanisms were ascertained by standard

techniques of geometry characterization, frequency tests and IRC as well as minimum energy reaction path (MERP) following.[13] In some cases that looked more sensitive than others (*e.g.*, the frontside saddle point in Fig. 3 later) several IRC options were used to verify the mechanistic identity. Basis set superposition errors (BSSEs) were calculated and found to be very small. For $C_2H_6^{\bullet+}$, the study was limited to the ET mechanisms of the isomer with the long C–C bond.[14–16]

ET mechanisms were searched along a reaction coordinate that leads to ET products. Using this approach we identified concerted-ET mechanisms for the $C_2H_6^{\bullet+}/H_2S$ and $C_2H_6^{\bullet+}/PH_3$ combinations. Whenever the concerted mechanism turned out to be barrierless, we located a structure of electron switch (e-switch); that is the location at which the wavefunction changes its character from reactant-like to ET-like *en route* to the ET product. This e-switch structure was located in the same manner as the concerted-ET saddle point. For example, the $C_2H_6^{\bullet+}/H_2S$ combination gave a barrierless concerted-ET at the UMP2 level. The corresponding e-switch structure was found starting at R(C–C) = 1.920 Å (the UMP2 optimized distance for the cation radical), and optimizing all other parameters. The procedure resulted in R(S–C) = 2.519 Å. Shortening the C–C distance to 1.90 Å and repeating the process resulted in the C–S distance going to infinity. Therefore, the e-switch structure is typified by R(C–C) = 1.920 Å and R(S–C) = 2.519 Å, the latter being the shortest distance possible between the cation radical and nucleophile.

Despite numerous searches in all other nucleophile/cation radical combinations, we could not find saddle points that connect *directly* the reactant- and ET product-clusters. Instead, the reactions were found to follow stepwise-ET mechanisms; later referred to as *shuttle-ET mechanisms*. In two systems, $NH_3/C_2H_6^{\bullet+}$ and $PH_3/C_2H_6^{\bullet+}$, there does not exist a reactant cluster in the backside trajectory and the energy of the system goes down from reactants toward both the nucleophilic substitution- and ET-product clusters. To establish a reaction mechanism for these systems, we performed a detailed grid of the potential energy surface starting from the reactant state [R(C–C) = 1.976 Å, R(Nu–C) = 5 Å]. The grid involved C–C and Nu–C distances as well as pyramidalization angle of the nucleophile; all other parameters were optimized. The grid provided the steepest descent pathway from the reactant state. This minimum energy reaction path (MERP) was found to involve an initial encounter of the nucleophile and the cation radical followed by a subsequent nucleophilic substitution or ET pathways (see later Fig. 6).

To obtain concerted transition state structure alternatives for the cases that exhibited stepwise shuttle-ET mechanisms, we searched for outer-sphere saddle points as well as crossing point structures that correspond to the Marcus–Hush[17] transition state models for ET reactions. Outer-sphere ET transition states could be located along pathways which impose *avoidance of bonding between the active orbitals of the two reactants.*[18] For example, in the case of the $NH_3/C_2H_6^{\bullet+}$ system, a saddle point was located along a trajectory in which the nucleophile is oriented with its three hydrogen atoms pointing toward the cation radical. This orientation prohibits any overlap between the lone-pair of the nucleophile and the σ orbital of the cation radical.

Crossing point structures (CPSs) were searched for the reaction, $C_2H_6^{\bullet+}/H_2O \longrightarrow C_2H_6/H_2O^{\bullet+}$. Each CPS corresponds to the geometry where two UHF solutions[19]—one having the spin localized on the C_2H_6 moiety and the other with the spin localized on the nucleophile portion—possess equal energy to within ≤0.02 kcal mol^{-1}. Two different stable localized UHF solutions could be generated by altering the guess and/or by using different SCF acceleration procedures (the two SCF solutions are not mixed by CI due to the Brillouin theorem).

The CPS itself was located by an iterative procedure which results in the species of the lowest energy. In each cycle the two localized structures were separately optimized and their 'crossing point' was found. For example, the lowest energy CPS was located along the trajectory of maximum overlap between the active orbitals (see **6** later). The first cycle involved a C–C distance reaction coordinate, while all the remaining parameters were optimized. This cycle provided a situation where the two structures possess equal energies but non-identical geometries. The two UHF solutions corresponding to this first 'false crossing point' were again traced along a different reaction coordinate and a new 'crossing point' was found, and so on. The procedure was terminated when the two UHF solutions were found to have the same energy for the *same geometric parameters.* The behaviour of this CPS was tested by single point calculation at the QCISD(T) level which showed that the two solutions are indeed very close in energy, and by CASSCF calculation which revealed an energy cusp and a switch of the character of the wavefunction in the CPS region. As shall be seen there exists a fundamental reason for the absence of a saddle point for the concerted ET process in this case.

Reliability of the computational trends

UHF and UMP2 calculations may not always be reliable because of their propensity for spin contamination and tendency to exaggerate the extent of spin-polarization. However, these problems do not appear to be severe in the present systems as could be deduced from the $\langle S^2 \rangle$ values which were consistently low, <0.77 (and 0.75 after first projection), indicating thereby only small spin-contamination. Nevertheless, to ascertain the validity of our mechanistic conclusions, we have carried out a full mechanistic search for the frontside mechanism of $H_2O/C_2H_6^{\bullet+}$ (Fig. 5) at the ROHF level of geometry optimization and IRC scans. With the exception of minor geometric and energetic differences, the resulting ROHF mechanism was virtually identical with the UHF mechanism.

A second type of test was carried out for the spin density and charge distribution which serve in this paper as mechanistic indicators (see later: structures **13** and **14**). Single-point ROHF calculation on **13** revealed that the ROHF densities are in full qualitative accord with the projected UHF (PUHF) and PQCISD(T) densities; the latter corrected to second order. A similar test on the species of the ET-shuttle mechanism in Fig. 5 led to the same conclusion that the ROHF and UHF densities are in full qualitative accord, as far as the mechanistic conclusions are concerned.

A third type of test was performed on the value of the vertical ET gap from the nucleophile to the cation-radical, which is a critical mechanistic parameter. Since the reaction of $H_2S/C_2H_6^{\bullet+}$ showed a worrisome sensitivity of this gap to the level of calculations (see later the first three entires in Table 1), it was decided to check the gap at the ROHF and ROMP2 levels. The results came out virtually the same as with the unrestricted calculations, UHF and UMP2. Thus, for UHF//UHF, the gap is 20.7 kcal mol^{-1} as compared with 21.8 kcal mol^{-1} for the corresponding ROHF level. The same gap is 5.11 kcal mol^{-1} at the UMP2//UHF level in comparison with 5.03 kcal mol^{-1} for the corresponding ROMP2 level. The root cause of the MP2 underestimation of this gap is the imbalanced treatment of the ionization potentials for the H_2S and C_2H_6 species. Thus, while UHF and ROHF perform equally badly for the two species and yield thereby correct ET gaps, the UMP2 and ROMP2 levels reproduce nicely the ionization potential of C_2H_6,[16] but underestimate the same quantity for H_2S. We tried several basis sets and found the same trend; the gap value is always underestimated at the MP2 level due to underestimation of the

ionization potential of H_2S. The same trend is observed at higher levels up to CCSD(T), and recurs for other nucleophiles like NH_3. *This indicates that correlated levels are not necessarily better for studying ET reactions, and HF levels will often be better because they treat the critical constituents of the ET gap in a balanced manner.* Furthermore, it is apparent that the sensitivity of the ET gap, to the level of calculation, is not an artefact of the unrestricted wavefunctions, but recurs also at the restricted levels. However since both UHF and UMP2 levels show that the ET reaction for the $H_2S/C_2H_6^{\bullet+}$ combination proceeds by a concerted ET mechanism, whatever imbalance there is in the MP2 treatment does not affect the mechanistic conclusions of this study.

Another technical point of concern is the extent of BSSEs which might affect the complexation energies in our potential energy profiles (Figs. 2–5). We point out that since our systems involve clusters of different electronic origins (*e.g.*, reactant clusters, ET clusters and proton transferred clusters; see Figs. 2–5), there is no way to define a standard BSSE for a given surface. Therefore, we estimated the BSSE value relative to the reactant clusters for three different reactions; $PH_3/C_2H_6^{\bullet+}$ (F), $H_2S/C_2H_6^{\bullet+}$ (F) and $H_2S/C_2H_6^{\bullet+}$ (B), and found BSSE values of 0.1 kcal mol^{-1}, 0.12 kcal mol^{-1} and 0.59 kcal mol^{-1}, respectively. A similar test for the ET cluster of the $PH_3/C_2H_6^{\bullet+}$ mechanism gave 0.29 kcal mol^{-1} as the corresponding BSSE. These results indicate that our systems do not exhibit large BSSEs even at the moderate basis set we use. However, this should not be taken as a general conclusion and BSSE values should be checked routinely.

In conclusion, our many computational tests in combination with the VB analysis of the problem provide us with some degree of confidence that the qualitative mechanistic schemes and principles that are derived in this paper should survive at more stringent levels of computations, when such levels become practical.

Results

Total energies and full geometrical details are collected in the form of a GAUSSIAN archive and are available from the authors.

Cation radicals

The long C–C bond structure of $C_2H_6^{\bullet+}$ is shown in Fig. 1, and is obtained by removing an electron from the a_{1g} σ(C–C)-type orbital.[14–16] Alongside the long-bond isomer of $C_2H_6^{\bullet+}$, we show the UMP2 structure[16] of the diboranoid isomer which possesses in-plane CCH_i angles smaller than 90°. This isomer is nascent from the ^2E_g vertical state of $C_2H_6^{\bullet+}$ where the electron is removed from the in-plane (H_iCCH_i) component-orbital of the degenerate e_g pair of orbitals of the parent C_2H_6 molecule. While we do not study the reactivity of this isomer as such, it is nevertheless shown in Fig. 1 because its characteristic structural feature, the acute in-plane CCH_i angle, is revealed in the ET mechanisms of the long bond structure.

Electron transfer mechanisms

The electron transfer mechanisms identified in this study are schematized by the reaction profiles in Figs. 2–5. These are continuous reaction profiles that connect all the critical species *via* IRC[13] and/or minimum energy reaction pathways (MERPs). Only principal skeletal parameters are indicated on the critical structures and the full details are available from the authors upon request. The designators (B) and (F) specify the trajectory of approach of the nucleophile to the cation radical, where (F) stands for frontside and (B) for backside in their usual meanings. The species representing minima are designated by the capitalized first letter of the species' name—R (reactants), P (products), C (cluster)—and a subscript which specifies the chemical nature of the species. Saddle point species are indicated by a letter specifying the chemical nature and superscribed by a dagger (*e.g.*, c-ET‡ means a concerted electron transfer type saddle point).

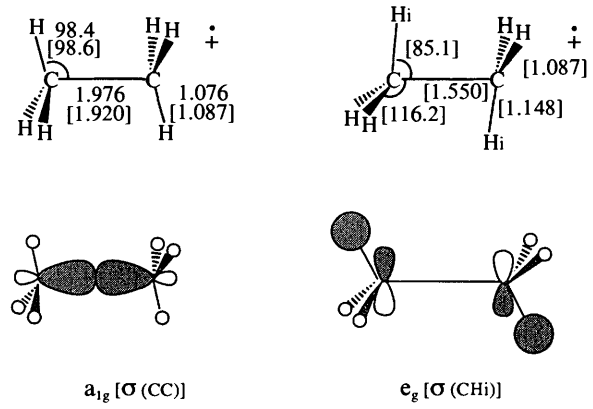

Fig. 1 UHF and UMP2 optimized structures (with 6-31G*) of $C_2H_6^{\bullet+}$. The figures in brackets are UMP2 values. The H_is are in-plane hydrogens of the diborane isomer of $C_2H_6^{\bullet+}$. Also shown are the C_2H_6 orbitals a_{1g} and e_g from which an electron is removed.

Concerted ET (c-ET) mechanisms

Fig. 2 shows the c-ET mechanisms for the $C_2H_6^{\bullet+}/PH_3$ combination. It is apparent that PH_3 transfers an electron to the cation radical in a concerted mechanism. Along the frontside trajectory we located a reactant cluster (C_R) followed by a saddle point (c-ET‡) that is connected directly to the electron-transferred cluster (C_{ET}) and to the exit channel at the ET product (P_{ET}). Inspection of the reaction vector mode of the saddle point shows that the motion is merely a swing of the PH_3 moiety from and to the midpoint of the C–C bond; and with a frequency of 66.2i cm^{-1}. This reaction vector mode is a conformational change from the cluster toward the saddle point. Since the saddle point structure shows virtually no electronic and skeletal reorganization, the barrier to the c-ET reaction is simply a conformational barrier. Indeed, along the backside trajectory, the MERP leads in a barrierless fashion to the ET cluster and further to the P_{ET} exit.

The asterisk in Fig. 2 signifies the structure at which the change in the wavefunction from R- to ET-like occurs *en route* to C_{ET}. This e-switch point corresponds to a species with a tight geometry, **1**, that shows that the c-ET mechanism is inner-sphere and follows the maximum overlap pathway.

Fig. 3 shows the c-ET mechanism found for the $C_2H_6^{\bullet+}/H_2S$ pair. The backside trajectory accords with our previous results[9] obtained with a basis set of a lesser quality. The reaction proceeds through a saddle point structure (c-ET‡) that is typified by a tight geometry and delocalized spin density; both features indicate the tightly bonded nature of this TS. At the UMP2 level of optimization, the c-ET‡ saddle point disappears and the process becomes a barrierless c-ET mechanism along the corresponding MERP that starts from the encounter species. At UMP2 too, *en route* to C_{ET}, the e-switch point corresponds to a tight structure, **2**, essentially resembling c-ET‡(B) that emerges from the corresponding UHF level. As explained in the methods section we favour the UHF results over the UMP2 results because of the gross underestimation of the vertical ET gap by the latter method. Be the profile as it may, it is apparent that despite the differences between the UHF and UMP2 profiles, they both lead to the same conclusion that ET takes place directly along a tightly bonded pathway.

Along the frontside trajectory in Fig. 3 we located another saddle point structure that connects directly the C_R and C_{ET}

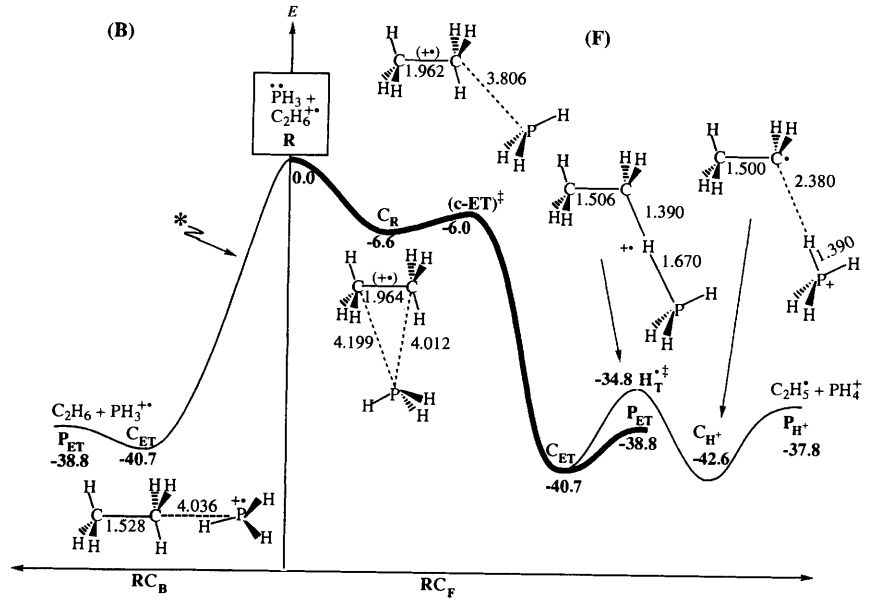

Fig. 2 Concerted ET (c-ET) mechanisms for $PH_3/C_2H_6^{\bullet+}$ in backside (B) and frontside (F) trajectories, at the UHF/6-31G* level. Energies in kcal mol^{-1} relative to the reactants (R) are shown near each species. The asterisk signifies the corresponding e-switch structure (**1**). Also presented is the hydrogen abstraction pathway starting from the C_{ET}, in the frontside trajectory [note: a bold line is used for the c-ET(F) mechanism].

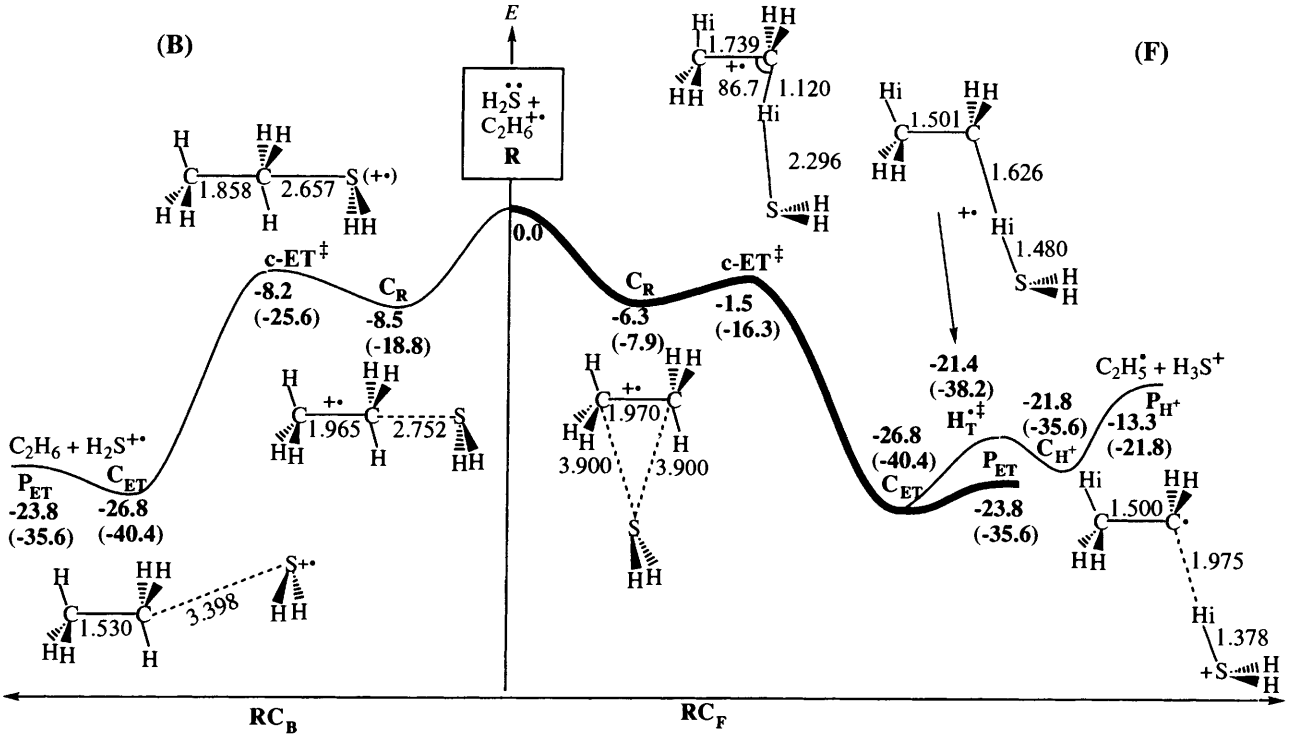

Fig. 3 Concerted ET (c-ET) mechanisms for $H_2S/C_2H_6^{\bullet+}$, at the UHF/6-31G* level. The figures in parentheses correspond to UMP2/UHF relative energies in kcal mol^{-1}. At the UMP2 level the c-ET mechanism is barrierless with an e-switch structure shown in **2**. Also presented is the hydrogen abstraction pathway starting from the C_{ET}, in the frontside trajectory [note: a bold line is used for the c-ET(F) mechanism].

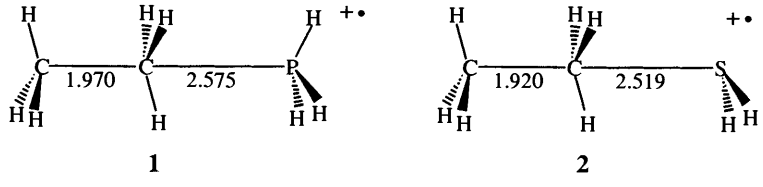

1 **2**

clusters. The outstanding structural feature of this c-ET‡ saddle point is the diboranoid feature (*cf.*, Fig. 1) of an acute CCH_i angle.

An interesting feature of the frontside trajectory, in both Figs. 2 and 3, is the hydrogen abstraction mechanism that is initiated from the electron transferred cluster. This process involves a

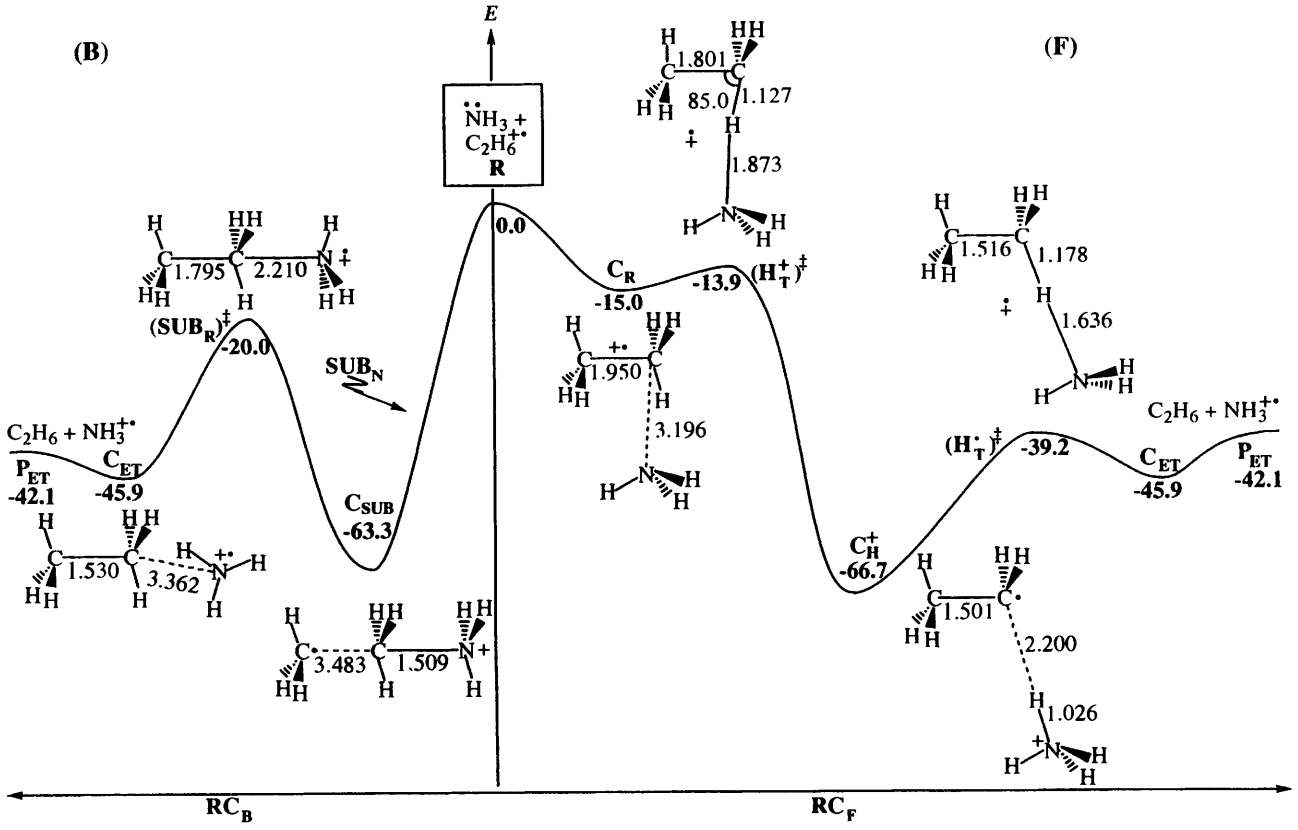

Fig. 4 Stepwise ET mechanisms for $NH_3/C_2H_6^{\bullet+}$ at the UHF/6-31G* level. The backside mechanism corresponds to the shuttle of the $Me^+/Me^\bullet$ redox pair (Me-shuttle). The frontside mechanism corresponds to the $H^+/H^\bullet$ shuttle (H-shuttle).

hydrogen abstraction saddle point $(H_T^{\bullet})^‡$ that connects C_{ET} to the proton transferred cluster (C_H^+) and products (P_H^+). Despite numerous attempts, we could not locate a direct proton abstraction pathway starting from either the reactants, $Nu:/RH^{\bullet+}$, or the corresponding reactant clusters.

In summary, the c-ET mechanisms of this study proceed along reaction profiles that are tightly bonded and are stereoselective. Following the terminology of references 1, 2(*a*), 2(*d*), based on Littler's definitions,[20] these bonded ET mechanisms are inner-sphere, as opposed to outer-sphere which should be very weakly bonded (by $\leqslant 1$ kcal mol^{-1}).

Stepwise ET shuttle mechanisms

Fig. 4 depicts the ET mechanisms of the $C_2H_6^{\bullet+}/NH_3$ pair along the MERPs of the backside and frontside trajectories. Starting from the reactants, R, it is seen that NH_3 transfers an electron to the cation radical in an indirect stepwise manner *via* two distinct mechanisms. Along the backside trajectory (to the left-hand side) the reactants undergo first a barrierless nucleophilic substitution process (SUB_N). The substitution cluster, C_{SUB} undergoes then a radical-type substitution (SUB_R) process *in the reverse direction* leading thereby to C_{ET}, *en route* to the electron transfer products exit channel, P_{ET}. Thus the ET process is brought about by a methyl group that shuttles back and forth as a redox pair $Me^+/Me^\bullet$ and as such transfers a single electron from the nucleophile to the cation radical; hereafter referred to as the Me-shuttle mechanism.

Yet another shuttle mechanism operates in the frontside trajectory of Fig. 4 (on the right-hand side). Here, an initial reactant cluster undergoes first a proton abstraction process (H_T^+) to form the corresponding cluster, C_{H^+}. In a subsequent step the ammonium ion moiety *gives back* a hydrogen atom to $C_2H_5^\bullet$ and generates the electron-transferred cluster and products. Thus, in this mechanism there occurs a shuttle of the redox pair $H^+/H^\bullet$ that results in a net electron transfer from NH_3 to the cation radical; hereafter referred to as the H-shuttle mechanism. Note that the diboranoid feature (angle CCH $< 90°$) appears now in the saddle-point structure $(H_T^+)^‡$ for the proton transfer step, whereas in Fig. 3 the same feature characterizes the saddle point for the concerted c-ET(F) process.

The ET mechanisms found at the UMP2 level of optimization for the $C_2H_6^{\bullet+}/H_2O$ pair are described in Fig. 5. It is important to recognize that an ET process in this case is feasible only in the exothermic direction, *i.e.*, $C_2H_6/H_2O^{\bullet+} \longrightarrow C_2H_6^{\bullet+}/H_2O$. Nevertheless to keep a uniform discussion we describe the mechanism starting from the cation radical/nucleophile combination, $C_2H_6^{\bullet+}/H_2O$. In this case both the backside and the frontside processes are stepwise ET mechanisms transpiring from the $H^+/H^\bullet$ redox pair shuttle. The only difference is that whereas in the frontside trajectory the proton transfer step has no saddle point, along the backside trajectory there exists a corresponding saddle point. This saddle point structure $(H_T^+)^‡$ possesses the diboranoid feature of an acute CCH angle, already noted in Figs. 3 and 4. At the UHF and ROHF levels (not shown in Fig. 5) both the backside and frontside trajectories possess $(H_T^+)^‡$ saddle points in the corresponding H-shuttle mechanisms.

Concerted *vs.* shuttle-ET mechanisms

To highlight the mechanistic distinction between the concerted- and H-shuttle ET mechanisms, we turn back to the frontside mechanisms present in Fig. 2 and Fig. 3 for the H_2S and PH_3 cases. It is seen that in each one of these cases, the proton abstraction cluster (C_{H^+}) does not originate directly from the reactants, but follows from the ET cluster that is the initial

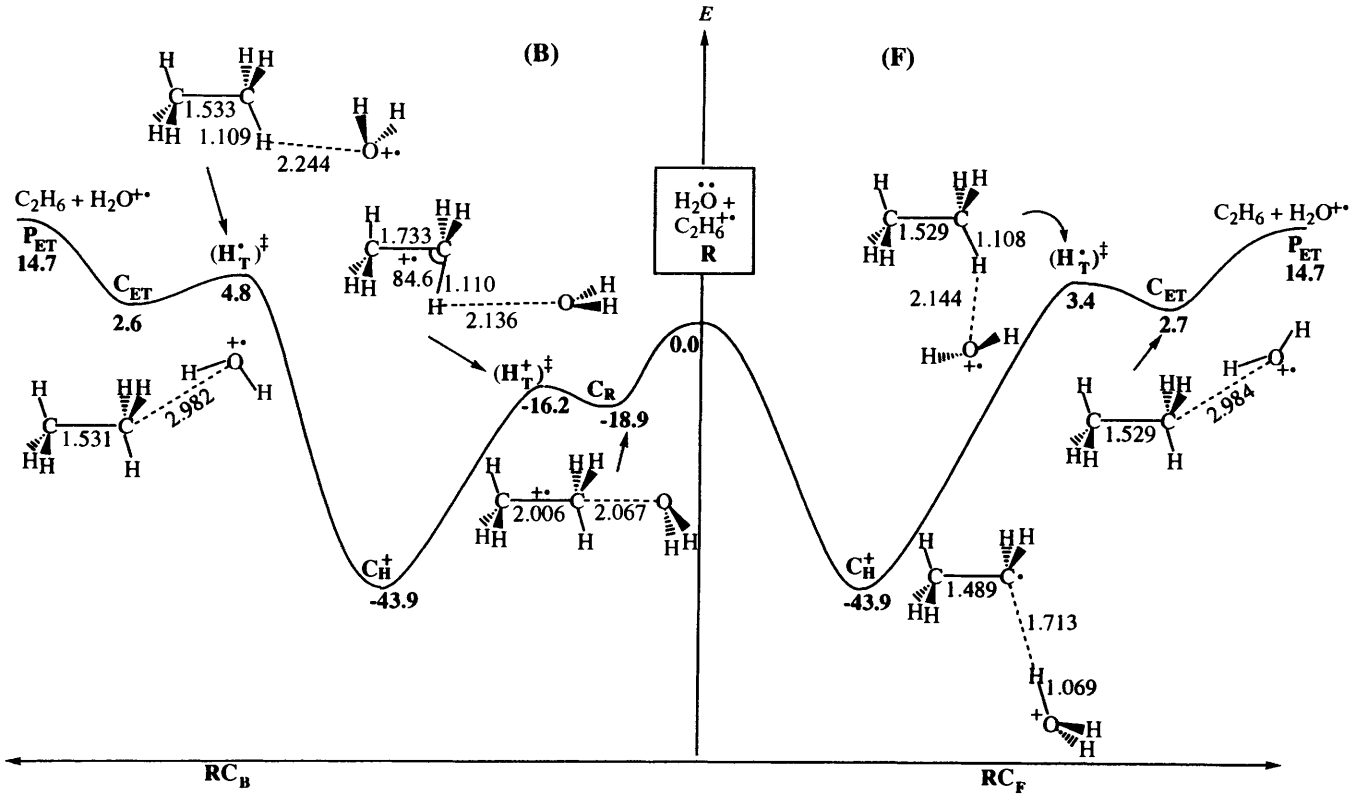

Fig. 5 Stepwise ET mechanisms (H-shuttle) for $H_2O/C_2H_6^{\bullet+}$ at the UMP2/6-31G* level

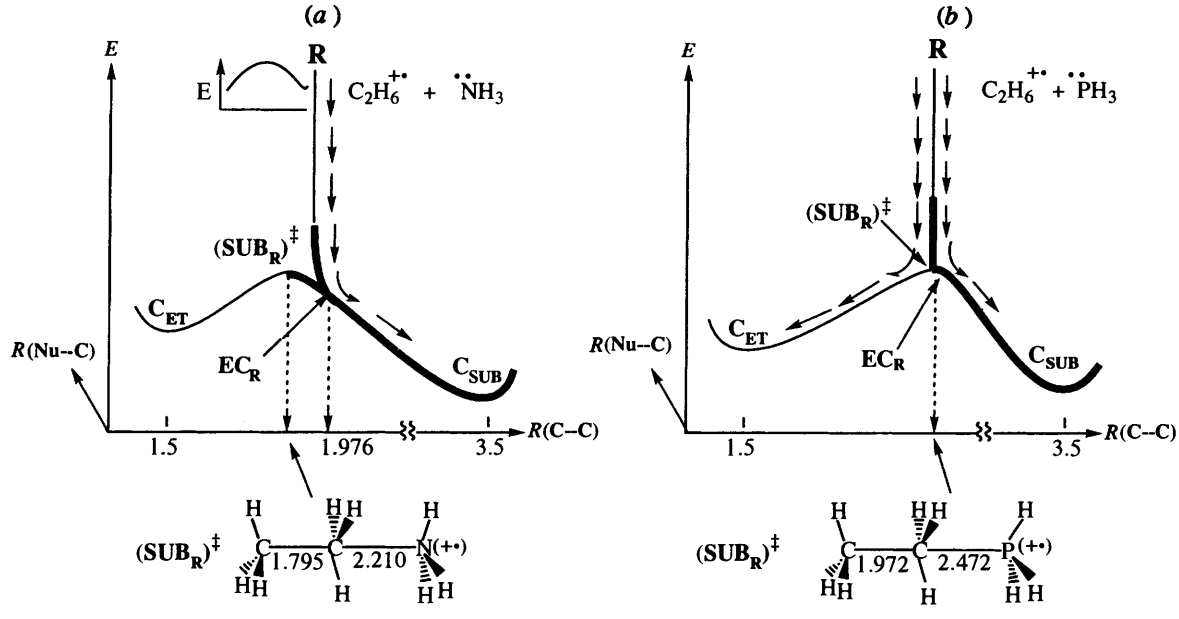

Fig. 6 Minimum energy reaction pathways (MERPs) starting from the reactant state R. The bold part of the profile comes towards the viewer in the direction of the short Nu–C distance. EC_R is the encounter 'complex' between the reactants. (*a*) The encounter complex continues to C_{SUB} because $SUB_R^{\ddagger}$ has a short C–C bond. The little profile near the R state indicates the energy change along the C–C shortening direction. (*b*) The encounter complex is distributed between C_{ET} and C_{SUB}.

product of the reaction. This is in stark contrast with the H_2O and NH_3 cases where the ET cluster is produced from the initially formed proton abstraction cluster.

Fig. 6 is a schematic projection of the multidimensional potential energy surface of the c-ET and Me-shuttle mechanisms based on a detailed energy grid. The only distance that is shown explicitly is the *R*(C–C) distance in the cation radical moiety. The other important distance for each species is *R*(Nu–C) that is not specified explicitly, and should be obvious from the properties of the species. Thus, C_{SUB} possesses a short Nu–C distance, while C_{ET} has a long distance. To indicate this information the branch of the energy profile that connects the $SUB_R^{\ddagger}$ saddle point to C_{SUB} is drawn with a bold line, while the other branch is drawn with a thin line. Similarly, the line that descends from the reactant state starts out thin to indicate long Nu–C distance and continues bold to indicate the decrease of this distance.

The arrows in the figure indicate the MERPs that are found in

the study starting from the reactant entrance channel. In both parts (*a*) and (*b*) the reactant state rolls down to an encounter complex species (EC_R) that is typified by a short Nu–C distance and a C–C distance equal to 1.976 Å; the initial value in the reactant cation radical. The encounter species resides, in turn, on the energy profile of the SUB_R process in between the ET and SUB clusters, and somewhere near the $SUB_R^{\ddagger}$ saddle point.

In Fig. 6(*a*) the $SUB_R^{\ddagger}$ saddle point possesses an *R*(C–C) distance (1.795 Å) that is significantly shorter than in the encounter species (1.976 Å). Consequently, the encounter species will face a barrier in the C–C shortening direction. As symbolized by the little energy profile near the reactant state, the energy increases in the C–C shortening direction, and this is true for any distance between the nucleophile and the cation radical. There exists therefore, an energy ridge—albeit low—that separates the encounter coordinate from the C–C shortening coordinate. Another ridge that exists initially at the C–C lengthening direction fades gradually as the Nu–C distance decreases. This double ridge creates, in turn, a steepest descent corridor that guides the reactant state down to the nucleophilic substitution cluster. The Me-shuttle ET mechanism will then be completed by crossing the $SUB_R^{\ddagger}$ saddle point on the SUB_R profile in the C_{ET} direction.

Fig. 6(*b*) shows the situation for the $PH_3/C_2H_6^{\bullet+}$ combination. Here the encounter species coincides virtually with the $SUB_R^{\ddagger}$ saddle point that acts therefore as a bifurcation point. Thus, continuing the C–C shortening mode will lead downhill to the ET cluster, C_{ET}, in a concerted ET mechanism, while a C–C lengthening will lead to C_{SUB} and a consequential Me-shuttle mechanism.

The location of the $SUB_R^{\ddagger}$ saddle point depends on the exothermicity of the process $C_{ET} \longrightarrow C_{SUB}$: the more exothermic it is the shorter the C–C bond in the respective saddle point. This is the reason why the $SUB_R^{\ddagger}$ saddle point of the $PH_3/C_2H_6^{\bullet+}$ combination possesses a longer C–C distance in comparison with the corresponding saddle point of the $NH_3/C_2H_6^{\bullet+}$ combination. As the $SUB_R^{\ddagger}$ saddle point moves to longer and longer C–C distances, the encounter species (EC_R) will be located on the left hand shoulder of the SUB_R profile and its MERP will be exclusively a c-ET mechanism. Such a situation occurs for the $H_2S/C_2H_6^{\bullet+}$ combination at the UMP2 level.

It is apparent therefore that Me-shuttle and c-ET are competing mechanisms that are available to $Nu:/C_2H_6^{\bullet+}$ combinations for which both the ET and SUB_N pathways are exothermic. If the reactant state can follow the MERP, then there will be a mechanistic selectivity, as in Fig. 6. However, when excess energy becomes available both the Me-shuttle mechanism and the c-ET mechanism will be accessed by the reactants.

An interesting observation in our study is the fact that for quite a few systems that have been investigated, there exist a maximum of two saddle points that connect reactants, ET- and SUB-products. Thus, whenever both c-ET‡ and $SUB_N^{\ddagger}$ exist, as in the $H_2S/C_2H_6^{\bullet+}$ system at the UHF level,[9] the third saddle point $SUB_R^{\ddagger}$ could not be found on the potential energy surface. This latter saddle point appeared only in those systems where the SUB_N and c-ET pathways are barrierless as in Fig. 6. This finding appears quite reasonable, because with two reaction coordinates available (C–C and Nu–C) we may not expect more than two saddle points. In solution, however, the solvent adds an additional degree of freedom (solvent reorganization coordinate) and we may expect situations where all the saddle points will coexist in the potential energy surface.

Outer-sphere ET alternatives for stepwise ET-shuttles

Having established the nature of the shuttle mechanisms, we turned to alternative c-ET pathways. Such alternatives turned out to be the outer-sphere saddle points which connect reactants and ET products directly. The outer-sphere saddle points for ET reactions of NH_3 with $C_2H_6^{\bullet+}$ and of PH_3 with $C_2H_6^{\bullet+}$ are shown, respectively in **3** and **4**, both of which lie above the reactants' entrance channel (by 2.9 kcal mol^{-1} and 0.3 kcal mol^{-1}, respectively). It is apparent that these saddle point structures represent trajectories that *prohibit bonding* between the nucleophile and the cation radical moiety. Once the constraints are removed, the MERP takes over and results in Me-shuttle and c-ET mechanisms, respectively. *Thus, 'avoided bonding' is the only way to effect a direct ET whenever the MERP has a shuttle-ET pathway available to it.* Moreover, the relative energy of the outer-sphere saddle point **4** for the $PH_3/C_2H_6^{\bullet+}$ system, and the related inner-sphere point in **1** is 12.3 kcal mol^{-1} in favour of the inner-sphere structure, and this is a clear demonstration of the inherent preference of c-ET for maximum bonding pathways.

To explore other options for concerted ET alternatives, we have also located crossing point structures (CPSs) which are the transition state models in the Marcus–Hush treatment[1,2,17] of concerted ET reactions. Two CPSs were located for the $H_2O/C_2H_6^{\bullet+}$ combination and are shown in **5** and **6**. The CPS in **5** involves a hydrogen-bonded trajectory originating from the ET cluster C_{ET} in Fig. 5. The large distance between the two reactants in **5** and the lack of any significant overlap between the active oribitals qualify this CPS as an outer-sphere structure. The CPS in **6** involves weak overlap of the H_2O lone pair with the σ-type orbital along the C–C axis, and is found to be significantly more stable than **5** (by 13.8 kcal mol^{-1}). However, the longer O–C distance in **6** in relation to the corresponding reactant cluster (C_R in Fig. 5) is a testimony that bonding is rather weak in this CPS too.

Fig. 7 highlights the disadvantage of the outer-sphere saddle points relative to the bonded mechanisms, by using the reactions of $C_2H_6^{\bullet+}/PH_3$ and $C_2H_6^{\bullet+}/NH_3$ as prototypes. Thus, Fig. 7(*a*) compares the energetic situation of the outer-sphere ET saddle point (**4**) to the c-ET bonded mechanism of $C_2H_6^{\bullet+}/PH_3$, and to the tight e-switch point **1** that was identified on this profile. Fig. 7(*b*) compares the outer-sphere ET saddle point (**3**) to the Me-shuttle mechanism of $C_2H_6^{\bullet+}/NH_3$. Precisely the same relationship as in Fig. 7(*b*) applies also to the CPSs **5** and **6** in comparison with the profile of the H-shuttle mechanism in Fig. 5. It is clear that all these weakly bonded outer-sphere structures lie higher in energy than the critical structures of the bonded ET mechanisms. This trend highlights the overwhelming role of bonding in the ET processes. Thus, from the point of view of the potential energy surfaces, *the outer-sphere ET is not a preferred mechanism; rather it is a default option.*

Though our main focus here is the potential energy surface view, we must also consider the reaction dynamics in any given situation. Thus, the outer-sphere structures in Fig. 7 do not lie very high above the reactant's entrance channel. Consequently, even though the bonded mechanisms are preferred from the point of view of the potential energy, the outer-sphere channel may be competitive with them especially under gas-phase conditions.

Discussion

Our model ET reactions are simplistic, but they nevertheless make a clear conceptual point about the intricate nature of the ET process. Two major questions then arise: what are the factors that determine the mechanistic choice of a given pair of cation radical and nucleophile, and what are the bonding principles that govern transition-state structures as well as the shapes and topologies of the energy profiles for ET mechanisms?

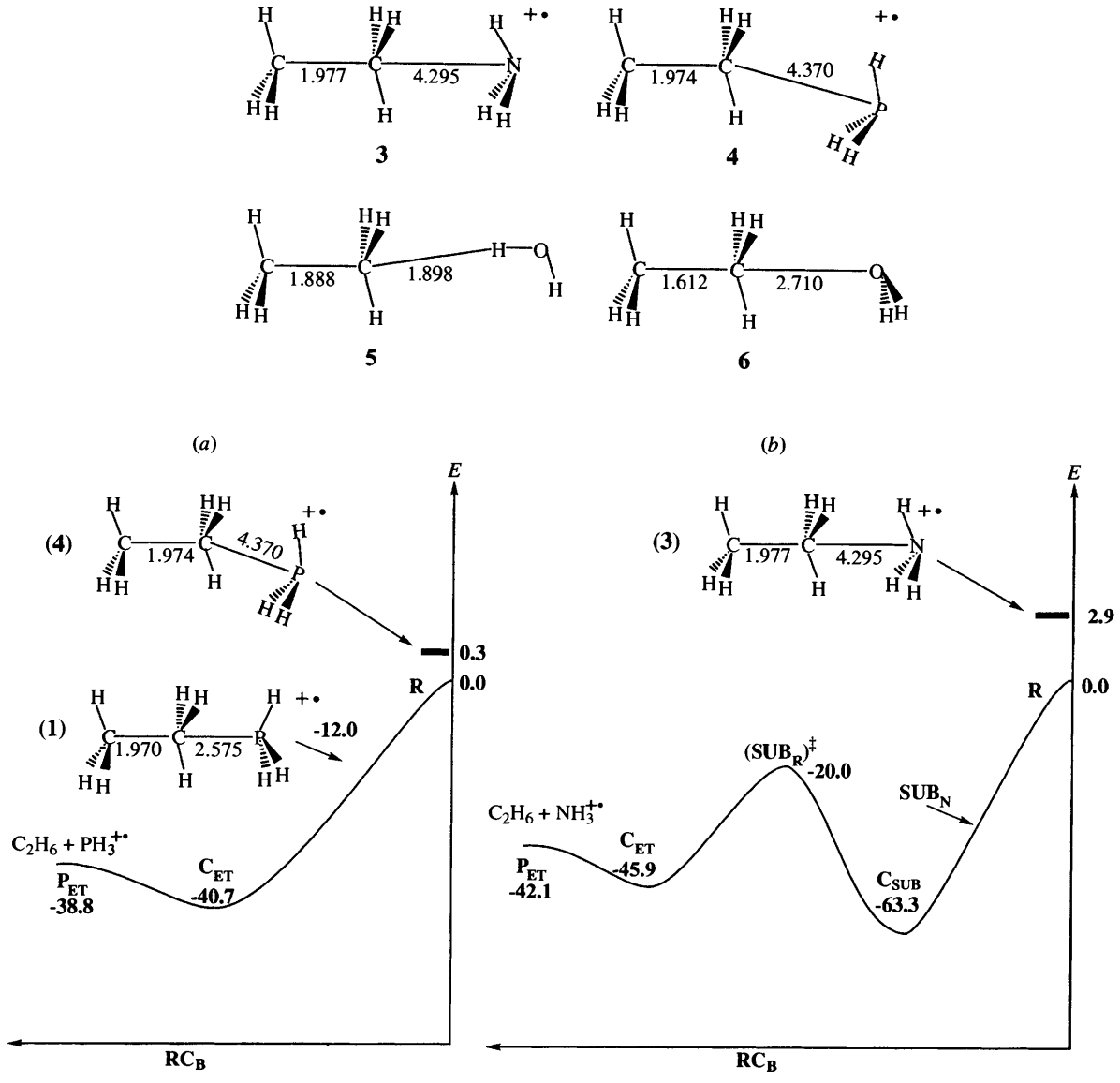

Fig. 7 Comparison of the bonded-ET profiles and the outer-sphere saddle points, for the backside ET mechanisms of (*a*) $PH_3/C_2H_6^{\bullet+}$ (from Fig. 2), and (*b*) $NH_3/C_2H_6^{\bullet+}$ (from Fig. 4). Also shown in (*a*) is the e-switch structure **1**. The energy values are in kcal mol^{-1}.

The origins of mechanistic ET manifold and variable TS character

Rate–equilibrium and thermochemical considerations. Thermodynamic principles are useful guides for rationalizing some gross features of the mechanistic choices. Table 1 collects the energetics for the overall ET reaction (ΔE_{ET}), the proton-transfer step [$\Delta E(H_T^+)$], and the substitution step (ΔE_{SUB}). It is apparent that, with the exception of $H_2O/C_2H_6^{\bullet+}$ where ET is endothermic, all other combinations have exothermic ET and can undergo this reaction easily. Similarly, the other two processes are exothermic for all the combinations, and one might expect therefore that all the systems will possess facile proton transfer and substitution steps as well. Indeed, the nucleophilic substitution reactions are facile, and for their detailed discussion the reader is referred to ref. 21.

The penultimate column in Table 1 also shows the vertical electron transfer energy gap (G_{ET}) in a Marcus–Hush curve crossing diagram for the concerted ET process. This gap together with ΔE_{ET} lead in the last column to the reorganization energies λ, which are required to estimate the barriers expected for a concerted ET process of a given Nu/cation radical pair.[17] Thus, it is clear from the ET parameters that the $H_2O/C_2H_6^{\bullet+}$ combination would be expected to possess a much higher barrier for the concerted ET, in comparison with all other $Nu:/RH^{\bullet+}$ combinations. These other combinations are all expected to possess very small barriers for c-ET.

While these gross features are clear, most of the subtle features found in this study cannot be rationalized by the data in Table 1. For example, the electron transfer parameters do not provide a clue to an understanding of the structure of the c-ET transition states, especially the differences between the c-$ET^{\ddagger}$(B) and c-$ET^{\ddagger}$(F) structures for the $H_2S/C_2H_6^{\bullet+}$ combination, in Fig. 3, and the relation of c-$ET^{\ddagger}$(F) and $(H_T^+)^{\ddagger}$. An even more intriguing question that does not find rationale in Table 1, is why do $H_2S/C_2H_6^{\bullet+}$ and $H_3P/C_2H_6^{\bullet+}$ possess no direct pathways between the reactants and the proton-transferred clusters (Fig. 3 and Fig. 2)?

That Table 1 is insufficient for rationalizing all our findings is understandable because the rate–equilibrium approach is basically a two-configuration analysis, whereas most organic reactions are generally affected by many configurations.[22] This is true even for the concerted ET reactions of this study, as implied already by the proton transfer-likeness of the c-$ET^{\ddagger}$(F) saddle point for the $H_2S/C_2H_6^{\bullet+}$ combination (Fig. 3). Thus, we are concerned here with variable transition-state character which is determined by a balance of a few contributing

Table 1 Thermochemical quantities[a] for concerted ET mechanisms, and for proton transfer and substitution reactions between Nu:/$RH^{\bullet+}$ pairs

Nu/$RH^{\bullet+}$	Level	ΔE_{ET}	$\Delta E(H_T^+)$	ΔE_{SUB}	G_{ET}[e]	λ[g]
$H_2S/C_2H_6^{\bullet+}$	HF//HF	−23.8	−13.3	−26.5	20.7	44.5
	MP2//HF	−35.6	−21.8	−35.0	5.1	40.7
	MP2//MP2	−35.1	−21.4	−34.4	0.8	35.9
	Exptl.	−21 ± 2[b]	−21.8 ± 2[c]	−34.5 ± 2[d]	16 ± 2[f]	37 ± 2
$PH_3/C_2H_6^{\bullet+}$	HF//HF	−38.7	−37.8	−53.9	22.4	61.1
	Exptl.	−41.0 ± 2[b]	−40.6 ± 2[c]	—	21.2[f]	61.8
$NH_3/C_2H_6^{\bullet+}$	HF//HF	−42.1	−58.4	−61.2	20.5	62.6
	Exptl.	−31 ± 2[b]	−55.6 ± 2[c]	−55.7 ± 2[d]	24 ± 2[f]	55 ± 2
$H_2O/C_2H_6^{\bullet+}$	HF//HF	10.8	−15.8	−23.0	57.8	47.0
	MP2//MP2	14.7	−23.8	−26.1	53.1	38.4
	Exptl.	26.5 ± 2[b]	−18.6 ± 2[c]	−19 ± 3[d]	63 ± 2[f]	36.5

[a] In kcal mol^{-1}. All ΔE quantities refer to the process from reactants to respective products. [b] Determined from ionization potentials E_i (vertical and adiabatic) which are taken from D. H. Au and M. T. Bowers in *Gas Phase Ion Chemistry*, ed. M. T. Bowers, Academic Press, New York, 1979, Vol. 2, ch. 9. [c] Determined by use of the following thermochemical equation: $\Delta E(H_T^+) = D_{CH} + E_i(H) - E_i^a(C_2H_6) - E_{pa}(NuH^+)$. Proton affinities are taken from Bowers (in *b*), and from B. J. Smith and L. Radom, *J. Am. Chem. Soc.*, 1993, **115**, 4885. $E_i^a(C_2H_6) = 11.5$ eV. [d] Determined by use of the following thermochemical equation: $\Delta E_{SUB} = D_{CC}(C_2H_6^{\bullet+}) - E_{mca}$; E_{mca} is the methyl cation affinity of the nucleophiles taken from: M. Meot-Ner, Z. Karpas and C. A. Deakyne, *J. Am. Chem. Soc.*, 1986, **108**, 3913. $D_{CC}(C_2H_6^{\bullet+}) = 49$ kcal mol^{-1}. [e] G_{ET} corresponds to the vertical ET energy from $Nu/RH^{\bullet+}$ to $(Nu^{\bullet+})^V/(RH)^V$, at frozen geometries. [f] Determined by the use of ionization potentials from *b* and the vertical attachment energy (E_a^V) of $C_2H_6^{\bullet+}$. The latter is given by: $E_a^V(C_2H_6^{\bullet+}) = -E_i^a(C_2H_6) + \Delta E_R(C_2H_6)$. $\Delta E_R(C_2H_6)$ is the reorganization energy of C_2H_6 attendant upon the change of geometry from the equilibrium values of the cation radical to those of the neutral molecule. [g] $\lambda = G_{ET} - \Delta E_{ET}$ and is the reorganization energy from relaxed ET products to the geometry of the reactants. The barrier expression based on the outer-sphere model is given by the Marcus equation $\Delta E^{\ddagger} = (\lambda/4)[(\lambda + \Delta E_{ET})/\lambda]^2 = (G_{ET})^2/4(G_{ET} - \Delta E_{ET})$.

configurations, and we need therefore to develop the VB configuration mixing (VBCM) approach to deal with the mechanistic manifold of ET processes.[22]

VB structures for describing the manifold of ET mechanisms. The minimum number of VB configurations which can describe the mechanistic scheme is shown in **7**–**12**. These structures do not mix with each other initially at infinite distance between the reactants. However, at finite distances all the configurations possess the same symmetry and can potentially mix into the wavefunction, leading thereby to ET mechanisms of variable transition state character. This, in a nutshell, is the basis for the mechanistic families which will be discussed below.

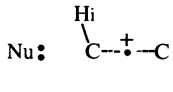

7, $\Phi_{R(CC)}$

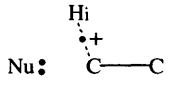

8, $\Phi_{R(CHi)}$

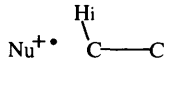

9, Φ_{ET}

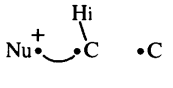

10, Φ_{SUB}

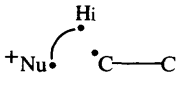

11, Φ_{Nu^+H}

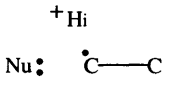

12, Φ_{NuH^+}

To maintain simplicity in the representation of the configurations, we depict only one of the C–H bonds for the $C_2H_6^{\bullet+}$ cation radical: an in-plane bond (hence, C–H_i). Structure **7** corresponds to the reactants' configuration, where the cation radical possesses a one-electron C–C bond, hence the label $\Phi_R(CC)$. Structure **8**, labelled as $\Phi_R(CH_i)$, is also a reactant configuration but now the cation radical state is localized in the in-plane C–H_i bonds, of which only one is shown. At infinite separation between the reactants, the two cation radical states correspond to $^2A_{1g}$ and ^2E_g. These are the electron-shift states[16] of the cation radical that are mutually related by an electron shift between the σ(CC) and the $\sigma(CH_i)$ orbitals depicted in Fig. 1. We note that when C–C is long, structure **8** lies above **7**, but as the C–C bond shortens along the ET reaction coordinate the two configurations eventually attain equal energy and will mix extensively.[16]

The third configuration in **9** is Φ_{ET} which describes the electron-transferred products. We note that this product configuration can be generated from either $\Phi_R(CC)$ or $\Phi_R(CH_i)$ by an electron transfer from the nucleophile to either the CC or the CH_i moieties of the cation radical. Structure **10** has a spin-pair between $Nu^{\bullet+}$ and the central carbon, and corresponds accordingly to the substitution configuration.

The remaining configurations **11** and **12** are the structures that describe the proton-transferred products, and by mixing they generate the state wavefunction of the $(Nu–H)^+$ bond and the $C_2H_5^{\bullet}$ radical. It is important to recognize that structure **12** originates from $\Phi_R(CH_i)$ since *this latter configuration has a major component where the positive charge is located on the in-plane hydrogens*, H_i, *as required by* **12**. On the other hand, structure **11** arises from further excitation of Φ_{ET} by unpairing the bonding electrons of the C–H_i.[23] This enables their pairing to the $Nu^{\bullet+}$ species, seen in **11**. As a consequence of this additional excitation, **11** is generally a high-energy structure.

Transition-state character in concerted ET mechanisms. Let us demonstrate first the multiconfigurational nature of the c-ET reactions of $H_2S/C_2H_6^{\bullet+}$. This can be done following our recent analyses[21,24] for obtaining the weights of the contributing VB structures from the charge and spin distributions of the transition states (see the Appendix). The projected UHF spin (ρ) and charge (Q) group densities for the c-ET‡(B) saddle point are shown in **13**. Similar density values (not shown) are obtained at the projected QCISD(T) level, as well as at the ROHF level. An important characteristic of the structure is the disparity of the spin and charge on the various groups in the transition state. Thus, the ratio $\rho(H_2S)/Q(H_2S)$ that is smaller than unity indicates that part of the spin density on $H_2S^{\bullet+}$ is paired up.[21] This in turn results from the mixing of the Φ_{SUB} into the crossing point of $\Phi_R(CC)$ and Φ_{ET}. Indeed using our method of VB analysis (see the Appendix)[21] we obtain the following

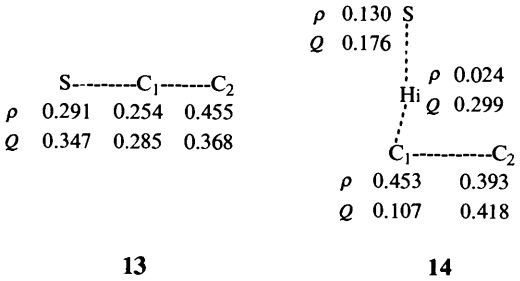

13

14

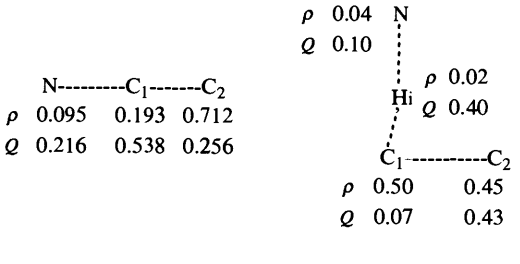

15

16

coefficients (*a*) for the contributing VB configurations to the wavefunction of c-ET‡(B).

$$a[\Phi_R(CC)] = 0.806\ (0.789) \quad (2)$$

$$a(\Phi_{ET}) = 0.421\ (0.455) \quad (3)$$

$$a(\Phi_{SUB}) = 0.237\ (0.253) \quad (4)$$

The parenthetical results correspond to the projected QCISD(T) wavefunction corrected to second order.§

It is seen that the reactant- and the ET-configurations are the major contributors to the wavefunction, but that the SUB configuration is also significant. Thus, c-ET‡(B) has a highly mixed VB character, much as in common tightly bonded organic transition states. A similar conclusion is derived by analysing the spin and charge density distribution in the e-switch structure for the barrierless process of $PH_3/C_2H_6^{\bullet+}$ (*cf.*, **1**). This multiconfigurational character that typifies the backside c-ET process is responsible for the strong bonding between the nucleophile and the cation radical along the reaction coordinate. Moreover, it follows that the concerted c-ET(B) mechanism *borrows a character of the nucleophilic substitution process*, itself being the first step in the $Me^+/Me^\bullet$ shuttle-ET mechanism.

In the frontside trajectory of $H_2S/C_2H_6^{\bullet+}$, the overlap between the lone-pair orbital of the nucleophile and the σ(CC) orbital of the cation radical is very poor (0.007). To maximize the overlap, the nucleophile goes to the in-plane hydrogen, and consequently $\Phi_R(CC)$ *is replaced* by $\Phi_R(CH_i)$ as the main reactant configuration. Thus, unlike c-ET‡(B) where all the Hs possess negative spin density, in c-ET‡(F) in **14** the in-plane hydrogens possess a positive spin density. This and the acute CCH_i angle of c-ET‡(F) are both indicators of $\Phi_R(CH_i)$—the parent configuration of the diboranoid isomer of $C_2H_6^{\bullet+}$.[16] A further indication for the replacement of $\Phi_R(CC)$ by $\Phi_R(CH_i)$ is the positive overlap population between the nucleophile and the in-plane hydrogen as opposed to the negative overlap population between the nucleophile and C_1: precisely the opposite of the overlap population patterns of c-ET‡(B). Thus, *the* c-ET(F) *mechanism involves an electron transfer from the nucleophile to the singly occupied* $\sigma(CH_i)$ *orbital of the respective bond.*

The multiconfigurational nature of c-ET‡(F) in **14** is apparent by the ratio $\rho(H_2S)/Q(H_2S) < 1$, as well as by the inverse nature of the ratio $\rho(C_1)/Q(C_1) > 1$. Thus, part of the spin density of $H_2S^{\bullet+}$ is paired up, while excess spin accumulates on C_1. These features are contributed by Φ_{Nu^+H} (**11**) and Φ_{NuH^+} (**12**); the latter is latent in $\Phi_R(CH_i)$ **8**. *It follows therefore that the* c-ET(F) *mechanism possesses proton transfer character.*

Transition-state character in the ET-shuttle mechanisms. Consider the Me-shuttle mechanism that was characterized for the backside trajectory of the $NH_3/C_2H_6^{\bullet+}$ system, in Fig. 4. Since the nucleophilic SUB_N process proceeds downhill without a saddle point, we show in **15** the spin and charge densities of one of the structures along this SUB_N pathway (with C–N and C–C distances being 2.2 and 2.1 Å, respectively). The small $\rho(NH_3)/Q(NH_3)$ ratio in **15** indicates that part of the spin on $NH_3^{\bullet+}$ is paired up, but part of it remains free. This situation results from the mixing of the Φ_{SUB} and Φ_{ET} configurations along the reaction coordinate. This is precisely what was found in our recent study of the nucleophilic substitution processes, which were all shown to involve ET character.[21] Indeed our VB analysis leads to the following coefficients (see the Appendix).¶

$$a[\Phi_R(CC)] = 0.872 \quad (5)$$

$$a(\Phi_{ET}) = 0.179 \quad (6)$$

$$a(\Phi_{SUB}) = 0.348 \quad (7)$$

It is apparent that the SUB_N *step of the shuttle mechanism for* NH_3 *involves* ET *character*, much the same as the concerted ET reaction of H_2S involves SUB character, both being multiconfigurational pathways related by the same contributing VB structures.

In **16** we depict the spin and charge densities for the proton transfer saddle point $(H_T^+)^‡$ in the $H^+/H^\bullet$ shuttle-ET mechanism of $NH_3/C_2H_6^{\bullet+}$. It is apparent that there is great similarity between this structure and the c-ET‡(F) structure in the $H_2S/C_2H_6^{\bullet+}$ case (**14**). Once again, the disparity of spin- and charge-density on the nucleophile indicates that part of the spin on $NH_3^{\bullet+}$ is paired up, but part of it remains free. This situation is an outcome of the mixing of Φ_{ET} character into the proton transfer saddle point. The same conclusion is obtained by inspecting the charge and spin distributions for the $(H_T^+)^‡$ saddle point in the $H_2O/C_2H_6^{\bullet+}$ combination. It is clear therefore that *the H-shuttle mechanism involves* Φ_{ET} *character mixed with* $\Phi_R(CH_i)$ *as well as with* Φ_{Nu^+H}, *and is related thereby to the concerted* ET(F) *process*, **14**, both sharing the same contributing configurations.

Genesis of ET mechanisms from the VB configuration set. The preceding discussion shows that the VB configurations fall into two distinct subsets that form building blocks of two mechanistic groups. These groups are depicted schematically as two connected triangles in Fig. 8. The right-hand triangle is made of the $\Phi_R(CC)$, Φ_{SUB} and Φ_{ET} which interchange along the respective reaction coordinates and form the c-ET(B) and the Me-shuttle mechanisms. The left-hand triangle is made of the $\Phi_R(CH_i)$, Φ_{ET} and $\Phi_{(NuH)^+}$ configurations; the latter configuration corresponds to a linear combination of Φ_{Nu^+H} (**11**) and Φ_{NuH^+} (**12**) that describe the $(NuH)^+/C_2H_5^\bullet$ proton-transferred

§ Not shown is the coefficient of $\Phi_{R^*}(CC)$ which is analogous to **7**, but having the odd electron occupied in the σ*(CC) orbital of the cation radical. The coefficient of $\Phi_{R^*}(CC)$ is 0.051.

¶ The coefficient of $\Phi_{R^*}(CC)$ is 0.156. A similar analysis of the $SUB_N^‡$ saddle point for the $H_2S/C_2H_6^{\bullet+}$ system in ref. 21 leads to the following coefficients: 0.840, 0.200, 0.400 and 0.092; for the reactant, ET, SUB and $\Phi_{R^*}(CC)$ configurations, respectively.

Table 2 Avoided crossing situations[a] and their corresponding elementary processes

Pairwise avoided[b] crossing	Orbital[c] mixing	Elementary process	Complementary mixing	Nu/RH$^{\bullet+}$ [h] combination
(1) $\Phi_R(CC)$, Φ_{ET}	n(Nu)–σ(CC)[c]	c-ET(B)	Φ_{SUB}	$H_2S/C_2H_6^{\bullet+}$(B), $PH_3/C_2H_6^{\bullet+}$(B)
(2) $\Phi_R(CC)$, Φ_{SUB}	n(Nu)–σ*(CC)[c]	SUB_N	Φ_{ET}	$NH_3/C_2H_6^{\bullet+}$(B)
(3) Φ_{SUB}, Φ_{ET}	*d*	SUB_R	$\Phi_R(CC)$	$NH_3/C_2H_6^{\bullet+}$(B)
(4) $\Phi_R(CH_i)$, Φ_{ET}	n(Nu)–σ(CH$_i$)	c-ET(F)	$\Phi_R(CC)$, Φ_{Nu^+H}	$H_2S/C_2H_6^{\bullet+}$(F),
(5) $\Phi_R(CC)$, $\Phi_R(CH_i)$	σ(CC)–σ(CH$_i$)			
(a) $\Phi_{(NuH)^+} \approx \Phi_{Nu^+H}$[e]	σ(CC)–σ(CH$_i$)	$C_2H_6^{\bullet+}$ (isomerization)	Φ_{NuH^+}, Φ_{ET}	
(b) $\Phi_{(NuH)^+} \approx \Phi_{NuH^+}$[f]	σ(CC)–σ(CH$_i$)	H_T^+	Φ_{Nu^+H}, Φ_{ET}	$H_2O/C_2H_6^{\bullet+}$ (B,F), $NH_3/C_2H_6^{\bullet+}$(F)
(6) $\Phi_R(CH_i)$, Φ_{Nu^+H}	n(Nu)–σ*(CH$_i$)	H_T^+	Φ_{ET}, $\Phi_R(CC)$	$H_2O/C_2H_6^{\bullet+}$(B,F), $NH_3/C_2H_6^{\bullet+}$(F)
(7) $\Phi_{(NuH)^+}$, Φ_{ET}	*g*	$H_T^{\bullet}$	$\Phi_R(CH_i)$	$H_2O/C_2H_6^{\bullet+}$(B,F), $NH_3/C_2H_6^{\bullet+}$(F), $H_2S/C_2H_6^{\bullet+}$(F), $PH_3/C_2H_6^{\bullet+}$(F)

[a] Three pairwise avoided crossings are not shown; (*i*) $\Phi_R(CC)$, Φ_{Nu^+H} contributes to H_T^+, (*ii*) $\Phi_R(CH_i)$, Φ_{SUB} corresponds to SUB_N starting from a diboranoid structure and (*iii*) Φ_{Nu^+H}, Φ_{SUB} corresponds to a coupled process, $(NuH)^+ + CH_3CH_2^{\bullet} \longrightarrow NuCH_3^+ + {}^{\bullet}CH_3$ (observed for $H_3O^+ + C_2H_5^{\bullet}$ at the UMP2 level). [b] The VB set is shown in **7**–**12**. [c] These orbital mixings correspond to the interactions of VB configurations that differ by a single electron shift. See references 23(*a*), (*b*). n(Nu) is the orbital of the nucleophile, *e.g.*, the NH_3 lone pair, *etc.* [d] This orbital mixing is proportional to the product of orbital overlaps [n(Nu)–σ(CC)][n(Nu)–σ*(CC)] and prefers therefore a backside trajectory. See similar analysis in reference 26 (footnote 12, 13 therein). [e] $\Phi_{(NuH)^+} = a\Phi_{Nu^+H} + b\Phi_{NuH^+}$ $a > b$. In this case, the $\Phi_R(CC)$–$\Phi_R(CH_i)$ avoided crossing will result in an isomerization of $C_2H_6^{\bullet+}$ to a diboranoid structure. [f] $b > a$ in the wavefunction in *e*. In this case, the $\Phi_R(CC)$–$\Phi_R(CH_i)$ avoided crossing will result in an H_T^+ process. [g] Starting from the C_H^+ cluster, the orbital mixing will involve the overlap of the radical centre $C_2H_5^{\bullet}$ with the σ and σ* orbitals of $(NuH)^+$. [h] The entries specify the $Nu/RH^{\bullet+}$ combination which proceeds *via* a given elementary process. Thus, for example, $NH_3/C_2H_6^{\bullet+}$(B) proceeds by the SUB_N and SUB_R steps; together corresponding to the Me-shuttle mechanism.

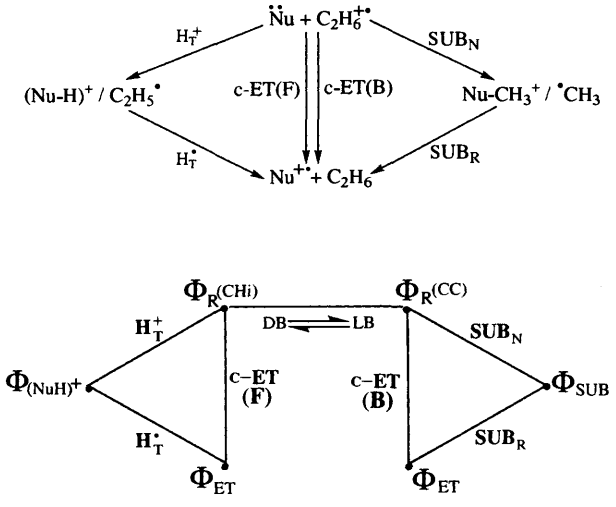

Fig. 8 The upper drawing shows the mechanistic manifolds and the lower drawing depicts the isomorphic interchange of the configuration building blocks. The right-hand triangle describes the concerted (c-ET) and Me-shuttle mechanisms, while the left-hand triangle describes the c-ET and H-shuttle mechanisms. A line connecting the VB configurations symbolizes a pairwise avoided crossing that generates a specified elementary process. The $\Phi_R(CC)$ and $\Phi_R(CH_i)$ avoided crossing corresponds to isomerization of the long (C–C) bond (LB) isomer of $C_2H_6^{\bullet+}$ to the diboranoid (DB) isomer.[16]

cluster. The interchange of the configurations specified in this left-hand triangle forms the c-ET(F) and H-shuttle mechanisms. It is seen from Fig. 8 that there is isomorphism between the configuration interchange and the chemical mechanisms, and this is the basis for the following discussion.

Table 2 provides the details of the genesis of the mechanistic groups and their electronic features from the VB building blocks **7**–**12**. The ground rules for using Table 2 follow from the avoided-crossing paradigm.[21–26]

Rule 1. An elementary process is generated by a pairwise avoided crossing. Table 2 lists seven of these, along with the nascent elementary process that each such pairwise avoided crossing potentially produces.

Rule 2. The mixing patterns of these pairs of configurations are determined by *matrix elements that provide structural selection rules for the elementary processes.* The simplest and most important mixing takes place between configurations that differ by a single electron shift. These configurations mix by optimizing the overlap between the orbitals that participate in the electron shift.[23b,25] More complex mixing situations[26] are relegated to the footnotes of Table 2.

Rule 3. Complementary configurations which can mix into a principal state, arising from a pairwise avoided crossing, will *endow the elementary process with complementary character.*

Rule 4. If two different pairwise avoided-crossing situations compete along the same reaction coordinate, the one with the lowest avoided-crossing state will determine the preferred mechanisms. The higher avoided-crossing state will correspond at best to a high-energy critical point.

Rule 5. A mechanistic family is formed by a group of coupled configurations whose cyclic permutation generates the concerted process and a particular stepwise pathway for the same process. These families are entries 1–3 and 4–7 in Table 2.

Let us turn now to discuss the mechanistic groups and choices of the target reactions between Nu: and $C_2H_6^{\bullet+}$, based on Rules 1–5.

The ET-SUB mechanistic group. The first mechanistic group, corresponding to the right hand triangle in Fig. 8, is formed by the three pairwise avoided crossings between $\Phi_R(CC)$, Φ_{ET} and Φ_{SUB} configurations; entries 1–3 (Table 2). The concerted ET (c-ET) mechanism transpires by $\Phi_R(CC)$–Φ_{ET} avoided crossing, while the Me-shuttle occurs *via* the sequential $\Phi_R(CC)$–Φ_{SUB} and Φ_{SUB}–Φ_{ET} avoided crossings. The three configurations are all coupled *via* orbital mixings which are substantial *only* in a collinear Nu–C–C backside arrangement.‖ Consequently, the c-ET process will involve SUB character in its wavefunction,

‖ The n(Nu)–σ(CC) overlap is 0.100 when the nucleophile approaches from the backside along the C–C bond axis, and only 0.007 when the nucleophile approaches from the frontside along the bisector of the C–C bond. The reason for this is that along the C–C axis the AO overlap is of σ-type, while along the bisector of the C–C bond the AOs are mutually perpendicular and possess very poor overlap.

through the mixing of Φ_{SUB} *via* the n(Nu)–σ*(CC) overlap. This is in fact what the configuration analysis shows for the $H_2S/C_2H_6^{\bullet+}$ system in eqns. (2)–(4). It is due to this excess bonding, endowed by the complementary mixing of Φ_{SUB}, that the c-ET process for PH_3 turns out to be barrierless, and much favoured in comparison with the outer-sphere process (Fig. 7(*a*); **1** *vs.* **4**). This is also the root cause why the Me-shuttle processes occur in Fig. 7(*b*) at much lower energy than any outer-sphere c-ET alternatives.

Much as c-ET contains complementary SUB character, the reverse is also true. Thus, the SUB_N process (entry 2) that arises from the elementary avoided crossing of the $\Phi_R(CC)$–Φ_{SUB} variety will contain ET character due to the complementary mixing of Φ_{ET}. Indeed, we recall from eqns. (5)–(7) that the H_3N–CH_3–$CH_3^{\bullet+}$ structures along the SUB_N path of the $NH_3/C_2H_6^{\bullet+}$ combination involve significant ET character. Similarly, the $SUB_R^{\ddagger}$ saddle point of the consecutive radical substitution process involves a H_3N–CH_3–$CH_3^{\bullet+}$ structure which arises from the elementary avoided crossing Φ_{ET}–Φ_{SUB} with complementary mixing of $\Phi_R(CC)$.

It is apparent therefore that, the three elementary processes in entries 1–3 are generated from three coupled VB configurations; $\Phi_R(CC)$, Φ_{ET} and Φ_{SUB}, and thereby constitute a mechanistic family of ET mechanisms that share multiconfigurational character defined by the constituent configurations. Since these configurations mix strongly and in a continuous fashion, it is very clear that the branches of the potential energy profiles that correspond to the two mechanisms will have common structures at which all the three elementary processes coalesce. These coalescence regions and the strong $\Phi_R(CC)$–Φ_{ET}–Φ_{SUB} mixing along the encounter geometry are responsible for the topology of the potential-energy surfaces discussed in Figs. 6(*a*) and 6(*b*) for the $NH_3/C_2H_6^{\bullet+}$ and $PH_3/C_2H_6^{\bullet+}$ cases. Indeed, the states of encounter species (EC_R) in Fig. 6 were found to possess a heavy mixture of the three VB structures, and to lack as such a unique configurational identity. This hybrid character makes EC_R the coalescence point at which the c-ET, SUB_N and SUB_R pathways all meet, and is therefore the strategic region in which the reactant state bifurcates between the c-ET and Me-shuttle mechanism.

In summary, the electronic structure of the transition states as well as the topologies of potential energy surfaces of the ET processes in *the ET-SUB mechanistic group, are all determined by the* Φ_R–Φ_{ET}–Φ_{SUB} *VB mixing and follow the maximum overlap principle.*

The ET–H_T mechanistic group. Let us turn back to Table 2 to the second group of configurations in entries 4–7. Entries 4, 5b, 6 and 7 show that the building blocks of the c-ET and the stepwise H-shuttle mechanisms are the pairwise avoided crossings between the $\Phi_R(CH_i)$, Φ_{ET} and Φ_{Nu^+H} configurations, with $\Phi_R(CC)$ providing a major complementary structure. This mechanistic group corresponds to the left-hand side triangle in Fig. 8.

The avoided crossing in entry 4 corresponds to an elementary process in which the electron is transferred from the nucleophile to the in-plane C–H_i bond. The selection rule associated with this avoided crossing is the n(Nu)–σ(CH_i) orbital overlap that prefers a frontside trajectory of approach of the nucleophile toward the H_i–C bond of $C_2H_6^{\bullet+}$ (*cf.*, the e_g orbital in Fig. 1). The complementary configuration in this case is $\Phi_R(CC)$, which adds an additional selection rule that may be read in entry 5a for the $\Phi_R(CC)$–$\Phi_R(CH_i)$ mixing. This mixing requires in turn overlap of the σ(CH_i) and σ(CC) orbitals; an overlap that is optimal only if the cation radical undergoes a diboranoid isomerization of the $C_2H_6^{\bullet+}$ moiety.[16] It follows that the complementary mixing of $\Phi_R(CC)$ into the avoided-crossing state of $\Phi_R(CH_i)$ and Φ_{ET} in entry 4 will endow the structure with a diboranoid distortion. In a similar fashion, the complementary mixing of Φ_{Nu^+H} into the saddle point in entry 4 will characterize it with a proton-transfer character. This type of c-ET(F)‡ saddle point with both proton-transfer and diboranoid character is computed for the $C_2H_6^{\bullet+}/H_2S$ combination in the frontside trajectory, *cf.*, Fig. 3.

Entries 5a and 5b further show that since Φ_{NuH^+} is the major character of $\Phi_R(CH_i)$, the outcome of the avoided crossing between $\Phi_R(CC)$ and $\Phi_R(CH_i)$ can also lead, under certain conditions, to proton transfer, depending on the nature of the $(Nu–H)^+$ bond, given by eqn. (8).

$$\Phi_{(NuH)^+} = a\Phi_{Nu^+H} + b\Phi_{NuH^+} \quad a^2 + b^2 = 1 \qquad (8)$$

Whenever the $(Nu–H)^+$ bond has major Φ_{NuH^+} character ($a < b$), as in entry 5b, the $\Phi_R(CC)$–$\Phi_R(CH_i)$ mixing, which is actually a $\Phi_R(CC)$–Φ_{NuH^+} avoided crossing, will result in a proton-transfer process with a diboranoid bending. However, when the $(Nu–H)^+$ bond has a major Φ_{Nu^+H} character ($a > b$), as in entry 5a, the $\Phi_R(CC)$–$\Phi_R(CH_i)$ mixing will contribute diboranoid bending of the cation radical. This dichotomy highlights the strong coupling between the c-ET(F) and H-shuttle mechanisms and provides the basis for understanding the mechanistic selection of a given $Nu:/C_2H_6^{\bullet+}$ pair between c-ET and H-shuttle, as discussed below.

$(Nu–H)^+$

Nu	*Q*(Nu)	*Q*(H)
H_2O	0.43	0.57
H_2S	0.73	0.24
H_3P	0.85	0.15
H_3N	0.52	0.48

17

Drawing **17** shows the charge distribution patterns at the UMP2 level for the $(Nu–H)^+$ bonds used in this study (a similar charge distribution is obtained at the UHF level). It is seen that the case of Nu ≡ H_2O represents the situation with major $Nu:H^+$ character, while the cases Nu ≡ H_2S and PH_3 represent the situation with major $Nu^{\bullet+}$ $^{\bullet}H$ character. A borderline case where the two situations are very strongly mixed is when Nu ≡ NH_3.

When the nucleophile is H_2O, two factors prefer a saddle point of the $(H_T{}^{\bullet})^{\ddagger}$ type to that of c-ET‡ type. First, owing to the dominant $H_2O{:}H^+$ nature of the $(H_2O–H)^+$ bond, the $\Phi_R(CC)$–$\Phi_R(CH_i)$ avoided crossing, which is $\Phi_R(CC)$–Φ_{NuH^+} type, and which occurs along the C–C shortening mode will result in a proton-transfer step as in entry 5b in Table 2. Second, due to the large ionization potential of the H_2O nucleophile, the $\Phi_R(CH_i)$–Φ_{ET} or $\Phi_R(CC)$–Φ_{ET} avoided crossings (entries 4 and 1), that compete with the proton transfer along the same C–C shortening coordinate, will create high energy structures (*e.g.*, CPS **6**). Following Rule 4, the $\Phi_R(CC)$–$\Phi_R(CH_i)$ avoided crossing will dominate the lowest energy mechanism along the C–C shortening coordinate, and will eventually generate the proton-transferred cluster, $(Nu–H)^+/C_2H_5^{\bullet}$. A subsequent avoided crossing of $\Phi_{(NuH)^+}$ and Φ_{ET} will cause $H_T^{\bullet}$ from $(Nu–H)^+$ back to $C_2H_5^{\bullet}$, and will complete thereby the H-shuttle mechanism on to the electron-transfer cluster. *Thus, poor donor ability of the nucleophile and dominant protium character of the* $(Nu–H)^+$ *bond will result in an H-shuttle mechanism.*

When the nucleophile is a good donor such as H_2S or PH_3, the relative energies of the avoided-crossing states will be inverted. First, $\Phi_R(CH_i)$–Φ_{ET} avoided crossing now provide a low-energy structure. Second, owing to the dominant $Nu^{\bullet+}$ $^{\bullet}H$ nature of the $(Nu–H)^+$ bond, the $\Phi_R(CH_i)$–Φ_{ET} avoided

crossing will simply endow the c-ET‡ saddle point with proton-transfer character and a diboranoid CCH_i angle (as in H_2S in Fig. 3).

Now we can also understand the puzzling results displayed in Figs. 2 and 3; namely that there do not seem to exist proton-transfer pathways which connect the reactants $H_2S/C_2H_6^{\bullet+}$ and $PH_3/C_2H_6^{\bullet+}$ to their proton transferred clusters, despite the exothermicity of these processes. Inspection of entry 6 in Table 2 shows that the only way to effect a proton transfer pathway in cases whose $(Nu–H)^+$ bond is dominated by the $Nu^{\bullet+}$ $^{\bullet}H$ character, is by means of the $\Phi_R(CH_i)$–Φ_{Nu^+H} avoided crossing that will have to compete with $\Phi_R(CH_i)$–Φ_{ET} avoided crossing along the same C–C shortening coordinate. Since the Φ_{Nu^+H} configuration is initially of very high energy (owing to the triplet nature of the electrons in the $C^{\bullet}$ $^{\bullet}H_i$ moiety in **11**) the $\Phi_R(CH_i)$–Φ_{Nu^+H} avoided crossing will create a high-energy critical structure. Following Rule 4, the lower-energy state associated with the $\Phi_R(CH_i)$–Φ_{ET} avoided crossing will win out and result in a c-ET process. This is the reason why these systems do not possess a direct pathway from the reactants to the proton-transferred clusters (Fig. 2 and Fig. 3). *Thus, nucleophiles which are good electron donors and possess* $(Nu–H)^+$ *bonds with low protium character are expected to proceed* via *c-ET mechanisms and to lack direct pathways from the reactants to the proton-transfer products.* These latter products will occur only after the ET step by $H_T^{\bullet}$ from NuH^+ to $C_2H_5^{\bullet}$ (see Figs. 2 and 3 frontside trajectories).

NH_3 as a nucleophile constitutes a borderline situation where the $(Nu–H)^+$ bond in **17** is described by almost equal amounts of the structures Φ_{NuH^+} and Φ_{Nu^+H}. While a clean prediction could not be made for this borderline case, nevertheless its preference (in a frontside trajectory) for a proton-transfer initiated shuttle-ET looks reasonable. This is so because the strong bonding along the proton transfer pathway may shift the saddle point and tip its character from c-ET‡(F) to $(H_T^+)^{\ddagger}$ type. It is entirely possible that substitution of NH_3 by better electron donors like CH_3NH_2 will make the $(Nu–H)^+$ bond more $Nu^{\bullet+}$ $^{\bullet}H$ type and will thereby tip back the saddle point in the c-ET‡(F) direction.

In summary, the electronic structure of the transition states as well as the topologies of potential-energy surfaces of the ET processes in the ET–H_T mechanistic group, are all determined by the Φ_R–Φ_{ET}–Φ_{Nu^+H} VB mixing and follow maximum overlap trajectories. This is the reason why the outer-sphere saddle points and crossing-point structures (*cf.*, **3**–**6**) are invariably higher than the bonded c-ET and H-shuttle pathways.

Experimental analogues and design of ET-mechanistic manifolds

Our study establishes the intricate nature of ET reactions between cation radicals and nucleophiles, and outlines with great detail the subtle relationships between the mechanistic members in a given manifold. While this detailed understanding is necessary to establish the ground rules of the model scheme, two questions should still be tackled albeit not fully answered. Are there any shuttle-ET mechanisms known? How should one design efficient ET-shuttles?

The H-shuttle mechanism can proceed in the gas phase in the exothermic direction, and therefore in cases like $H_3N/C_2H_6^{\bullet+}$ the ET products will be produced by proton transfer followed by a reverse H-atom transfer. However, in the H_2O case the exothermic direction is $H_2O^{\bullet+} + C_2H_6 \rightarrow \rightarrow H_2O + C_2H_6^{\bullet+}$. In this direction, the H-shuttle mechanism commences with a hydrogen abstraction from C_2H_6 by the $H_2O^{\bullet+}$ and follows with a protonation of the ethyl radical by H_3O^+. While these two steps may seem rather uncommon organic chemical mechanisms, both actually have precedents. Thus, the first step recurs in our computations for other systems as well (with PH_3 and H_2S, *cf.*, Figs. 2 and 3 above), and its simple experimental analogue is the hydrogen abstraction process from hydrocarbons by electronegative radicals. In the present case, the radical is the oxidized nucleophile $H_2O^{\bullet+}$. The second step in the reverse H-shuttle ET mechanism, the protonation of a radical, had already been postulated by Alder[27] as one of the components in an $S_{OE}1$ mechanisms. Thus, the constituent reactions of the H-shuttle are known. In fact, complete H-shuttles have been postulated by Whitten *et al.*[28] as quenching mechanisms in the reactions of triplet quinones and amines.

There are quite a few precedents to the ET-shuttle mechanisms which involve other group transfers. Thus, Davis and Gilbert[3d] investigated the reaction between strong oxidants and electron-rich olefins, and suggested a mechanism which involved addition of the oxidant (Ox) to the olefin RR'C=CXY to produce a radical RR'(Ox)C–CXY$^{\bullet}$ that subsequently underwent an oxidative cleavage of the C–Ox bond to produce the olefin cation radical, $RR'C{=}CXY^{\bullet+}$. This mechanism is the reverse process of the Me-shuttle mechanism in Fig. 4 [trajectory (B)]; starting with $C_2H_6/NH_3^{\bullet+}$ as the entrance channel and exiting at $C_2H_6^{\bullet+}/NH_3$. Other similar shuttle mechanisms have been proposed by Eberson *et al.*[3c,29] for reactions of aromatic cation radicals and nucleophiles in which the net ET process has been shown to occur by means of an addition–elimination mechanism whereby the nucleophile shuttles in and out and effects the reduction of the cation radical.

It is obvious that in solution-phase reactions, the shuttle mechanisms shown in Figs. 4 and 5 will not shuttle at all, but will be trapped in the thermodynamic sinks C_{SUB} and C_{H^+}. The fact that there exist experimental shuttle mechanisms[3,28,29] indicate that it should be possible to design ET-shuttles without the terminating sinks. What is required is to destabilize the sinks without eliminating them,§§ and at the same time keeping the overall ET process exothermic. This will flatten the entire potential-energy surface and will give rise to effective shuttle mechanisms.¶¶[,30]

In the case of the alkyl-shuttle mechanism [*e.g.*, Fig. 4, trajectory (B)], the sink C_{SUB} can be destabilized by increasing the degree of substitution of the cation radical,‖ ‖[,31] for a given nucleophile (*e.g.*, amine). This will weaken the Nu–C^+ bond and will destabilize the sink corresponding to C_{SUB}. The weakening of the Nu–C^+ bond will also facilitate the reverse radical substitution process, SUB_R, and consequently the entire potential-energy surface for the alkyl-shuttle mechanism will be flattened creating a feasible shuttle mechanism. Similar considerations may apply to modes of destabilizing the C_{H^+} sink for the H-shuttle mechanism, *e.g.*, by changing the proton affinity of the nucleophile. As mentioned above, for the H-shuttle mechanisms of NH_3, it is also possible to transform an H-shuttle mechanism to a c-ET mechanism, by modulating the protium (H^+) character of the $(Nu–H)^+$ bond *via* the ionization potential of the nucleophile. Another interesting possibility is the design of c-ET mechanisms with variable transition-state character, as discussed above. The possibilities are numerous and with appropriate thermochemical data it should be possible to construct a mechanistic manifold of complementary ET processes under realistic experimental conditions.

---

§§ The clusters are required to avoid consumption of the intermediate radicals, *e.g.*, by proton abstraction from the solvent, prior to the completion of the shuttle.

¶¶ We note the similarity of our conclusion to the strategy of Amatore *et al.*[30] to manipulate the efficiency of catalytic cycles ('A more efficient sequence would be one where the zero-valent species would be partly stabilized whereas the divalent intermediates would be destabilized . . .').

‖ ‖ It is important to emphasize that steric effects do not seem to slow down the SUB_N process to a significant extent as shown amply by Dinnocenzo *et al.*[31]

Conclusions

The present study is the first theoretical demonstration that ET—the simplest of all reactions—has potential-energy surfaces as complex and rich as most of the classical processes in organic chemistry. Thus, ET exhibits a manifold of mechanisms comprising concerted c-ET and stepwise ET-shuttle pathways. *The c-ET mechanisms involve saddle points or reaction pathways that occur along maximum overlap trajectories, and maintain strong bonding between the nucleophiles and the cation radicals. The stepwise mechanisms involve groups that shuttle back and forth as redox pairs* and transfer thereby an electron from the nucleophile to the cation radical. For all the cases there exist outer-sphere alternative saddle points and crossing point structures. These *outer-sphere structures are found along trajectories that avoid bonding between the nucleophile and the cation radical*, and are invariably higher in energy in comparison with the bonded ET-pathways, in one case by as much as 12.3 kcal mol^{-1} (**1** *vs.* **4**). Here and elsewhere,[9,32] we found *no computational evidence to justify an assumed*[2b] *dominance of the outer-sphere paradigm in organic ion radical chemistry.*

Two groups of complementary mechanisms are identified depending on the trajectory of approach of the nucleophile to the cation radical. The ET-SUB group is observed along the backside trajectory, and involves c-ET and Me-shuttle mechanisms [Figs. 2, 3 and 4, the (B) trajectory]. The ET-H_T mechanistic group is observed along the frontside pathway, and constitutes the c-ET and H-shuttle mechanisms [Fig. 4(F) trajectory and Fig. 5]. *The transition states in a mechanistic group are found to share electronic character, and hence also common structural features.*

A minimal set of five VB configurations can be used to conceptualize the mechanistic manifold and the variable electronic structures of the respective transition states. It is found that even the transition states of the c-ET processes possess multiple VB character, unlike the classical description in terms of two configurations. *It is this multiple VB character that confers strong bonding interactions between the nucleophile and the cation radical.* This is also the root cause for the variable transition-state structure in each mechanistic group. Thus, in the ET-SUB mechanistic group the saddle point for *the c-ET mechanisms contains the character of the substitution process* [eqns. (2)–(4)]. Similarly, in the stepwise Me-shuttle (see Fig. 4 for $C_2H_6^{\bullet+}/NH_3$), *the structures along the SUB pathway contain some character of the concerted ET process* [eqns. (5)–(7)]. In the ET-H_T mechanistic group *the various saddle points share ET as well as proton-transferred character.* This situation is reminiscent of the mechanistic manifold encountered in physical organic chemistry where many processes can occur *via* a family of related mechanisms, *e.g.*, the S_N2 and S_N1 mechanisms in the classical nucleophilic substitution process, or the E1, E2 and $E1_{CB}$ mechanisms in the 1,2-elimination process. The entire culture of variable transition-state approach in physical organic chemistry awaits to be brought to bear on mechanistic organic ET reactivity.

Our findings are not restricted to the $Nu:/C_2H_6^{\bullet+}$ system. Our on-going studies have revealed ET-mechanistic manifolds with variable transition-state structure in combinations such as, $Nu:/C_2H_4^{\bullet+}$, $Nu:/C_3H_6^{\bullet+}$, $Nu:/C_3H_8^{\bullet+}$, $Nu:/CH_3SiH_3^{\bullet+}$ and $Nu:/Si_2H_6^{\bullet+}$. *Evidently, organic ET reactions have very little resemblance to the pure ET reaction at the photosynthetic site and its analogues.*

Finally, the shuttle mechanisms discussed in this study bear resemblance to the inorganic ET processes mediated by ligand transfers. Thus, the Taube schemes[33] may ultimately find general support in organic reactions. In this respect, our results also suggest a way to unify the outer- and inner-sphere terminologies currently used with different meanings in organic and inorganic[1,20,34] ET reactions. We propose that the terms c-ET and shuttle-ET mechanisms be used to distinguish between direct ET reactions and those which require ligand- or group-transfers, irrespective of the inorganic or organic character of the reaction. Furthermore, to qualify the bonding of the ET-TS of c-ET mechanisms we suggest the use of the terms weakly bonded or structured.

Acknowledgements

This research is supported by the *Volkswagen Stiftung* and by the Israel Science Foundation Administered by the Academy of Sciences and Humanities. S. S. is thankful to T. W. Bally for a thorough reading and for enlightening discussions on computations of cation radicals.

Appendix

A model wavefunction for the backside reaction complex, $Nu–G_1–G_2$, has been recently constructed[21] from the configurations, $\Phi_R(CC)$, $\Phi_{R^*}(CC)$, Φ_{ET} and Φ_{SUB}. The $\Phi_{R^*}(CC)$ configuration involves an excited cation radical with the electron in the $\sigma^*(CC)$ orbital. Initially we construct a normalized linear combination of Φ_{ET} and Φ_{SUB}, in eqn. (A1). Here λ is the mixing coefficient of the Φ_{SUB} configuration, and the form of the normalization constant reflects the fact that the two configurations in eqn. (A1) share one common determinant. Since the two configurations involve an oxidized nucleophile, the linear combination is designated as $\Phi_{(Nu^+)}$. This wavefunction takes care of the charge–spin disparity on the nucleophile.

$$\Phi(Nu^+) = (1 + \lambda + \lambda^2)^{-\frac{1}{2}} [\Phi_{ET} + \lambda \Phi_{SUB}] \quad (A1)$$

The final wavefunction includes the mixing of $\Phi(Nu^+)$ with the remaining configurations in eqn. (A2). We then added to the wavefunction those parts which distribute spin and positive charge on the groups G_1 and G_2 of the cation radical.

$$\Psi = N[\Phi(Nu^+) + a_1\Phi_R + a_2\Phi_R^*]; \quad N = (1 + a_1^2 + a_2^2)^{-\frac{1}{2}} \quad (A2)$$

Translation of the coefficients of the wavefunction into group spin (ρ) and charge (Q) densities leads to λ in eqn. (A3).[21]

$$\lambda = 0.5 + 0.5\{[Q(Nu) + 3\rho(Nu)]/[Q(Nu) - \rho(Nu)]\}^{\frac{1}{2}} \quad (A3)$$

Using the expression for λ [eqn. (A3)] we obtain the following relationships between the group charges and spin densities of the $Nu–G_1–G_2$ reaction complex along the reaction coordinate, where the groups G are the CH_3 groups of the cation radical.

$$\rho(G_1) = Q(G_2) - \lambda[Q(Nu) - \rho(Nu)] \quad (A4)$$

$$\rho(G_2) = Q(G_1) + (1 + \lambda)[Q(Nu) - \rho(Nu)] \quad (A5)$$

Eqns. (A3)–(A5) are used to test the consistency of the wavefunction Ψ in eqn. (A2). First we use $Q(Nu)$ and $\rho(Nu)$ as input in eqn. (A3) to obtain λ. This λ value along with one pair of charge and/or spin density data are used as input for eqns. (A4) and (A5), which thereby provide the predictions for the missing pair of data. Extensive tests gave excellent fit with an accuracy of ρ and Q of better than 0.005e for a variety of systems. The accuracy of the predictions improved with improvement in the level of the computed wavefunction. In

general, projected wavefunctions give more accurate results than the unprojected ones, and the projected UHF level is comparable to the projected QCISD(T) level corrected to second order. Owing to these accuracy features of eqn. (A2), it was deduced that the wavefunction in this equation is consistent and can model faithfully the computed ρ and Q data.

Following these tests of consistency, the coefficients of the various configurations in the total wavefunction can be expressed as a function of the group charges and spin densities of the reaction complex in eqns. (A6)–(A9) that serve to obtain the weights of the configurations in eqns. (2)–(7) in the text.

$$a[\Phi_R] = 2^{-\frac{1}{2}}\{[Q(G_2)]^{\frac{1}{2}} + [Q(G_1)]^{\frac{1}{2}}\} \quad \text{(A6)}$$

$$a[\Phi_R{}^*] = 2^{-\frac{1}{2}}\{[Q(G_2)]^{\frac{1}{2}} - [Q(G_1)]^{\frac{1}{2}}\} \quad \text{(A7)}$$

$$a[\Phi_{SUB}] = [|Q(Nu) - \rho(Nu)|]^{\frac{1}{2}} \quad \text{(A8)}$$

$$a[\Phi_{ET}] = [|1 - Q(G_2) - \rho(G_2)|]^{\frac{1}{2}} \quad \text{(A9)}$$

References

1 L. Eberson, *Electron Transfer Reactions in Organic Chemistry*, Springer Verlag, Heidelberg, 1987.

2 (*a*) L. Eberson, *Adv. Phys. Org. Chem.*, 1982, **18**, 79; (*b*) J.-M. Saveant, *Adv. Phys. Org. Chem.*, 1990, **26**, 1; (*c*) J. K. Kochi, *Angew. Chem., Int. Ed. Engl.*, 1988, **27**, 1227; (*d*) L. Eberson, *New J. Chem.*, 1992, **16**, 151.

3 (*a*) L. Eberson, F. Radner and J. O. Svensson, *J. Chem. Soc., Chem. Commun.*, 1992, 114; (*b*) L. Eberson, *J. Chem. Soc., Perkin Trans. 2*, 1992, 1807; (*c*) L. Eberson and F. Radner, *Acta Chem. Scand., Ser. B*, 1984, **38**, 861; 1985, **39**, 357; (*d*) M. J. Davies and B. C. Gilbert, *J. Chem. Soc., Perkin Trans. 2*, 1984, 1809; (*e*) S. Steenken, *Chem. Rev.*, 1989, **89**, 503; (*f*) P. O'Neill, S. Steenken and D. Schulte-Frohlinde, *J. Phys. Chem.*, 1975, **79**, 2773; (*g*) V. Jagannadham and S. Steenken, *J. Am. Chem. Soc.*, 1984, **106**, 6542.

4 (*a*) R. A. More O'Ferrall, *J. Chem. Soc. B*, 1970, 274; (*b*) W. P. Jencks, *Chem. Rev.*, 1985, **85**, 511; (*c*) I. H. Williams, *Chem. Soc. Rev.*, 1993, **22**, 277.

5 J. A. Barnes, J. Wilkie and I. H. Williams, *J. Chem. Soc., Faraday Trans.*, 1994, **90**, 1709.

6 (*a*) D. Bethell, P. N. Clar and G. J. Hare, *J. Chem. Soc., Perkin Trans. 2*, 1983, 1889; (*b*) A. Pross, *Acc. Chem. Res.*, 1985, **18**, 212; (*c*) C. Perrin, *J. Phys. Chem.*, 1984, **88**, 3611.

7 J. P. Dinnocenzo, W. P. Todd, T. R. Simpson and I. R. Gould, *J. Am. Chem. Soc.*, 1990, **112**, 2462.

8 (*a*) S. F. Nelsen and J. T. Ippoliti, *J. Am. Chem. Soc.*, 1986, **108**, 4879; (*b*) J. P. Dinnocenzo and T. E. Bannach, *J. Am. Chem. Soc.*, 1989, **111**, 8646; (*c*) C. J. Schlesener, C. Amatore and J. K. Kochi, *J. Am. Chem. Soc.*, 1984, **106**, 7472.

9 J. K. Cho and S. S. Shaik, *J. Am. Chem. Soc.*, 1991, **113**, 9890.

10 M. J. Frisch, G. W. Trucks, M. Head-Gordon, P. M. W. Gill, M. W. Wong, J. B. Foresman, B. G. Johnson, H. B. Schlegel, M. A. Robb, E. S. Replogle, R. Gomperts, J. L. Andres, K. Raghavachari, J. S. Binkley, C. Gonzalez, R. L. Martin, D. J. Fox, D. J. Defrees, J. Baker, J. J. P. Stewart and J. A. Pople, GAUSSIAN 92, Revision C3, Gaussian, Inc., Pittsburgh PA, 1992.

11 M. W. Schmidt, K. K. Baldridge, J. A. Boatz, J. H. Jensen, S. Koseki, M. S. Gordon, K. A. Nguyen, T. L. Windus and S. T. Elbert, *QCPE Bull.*, 1990, **10**, 52, revision 11, March 1993.

12 P. C. Hariharan and J. A. Pople, *Theor. Chim. Acta*, 1973, **28**, 213.

13 C. Gonzalez and H. B. Schlegel, *J. Phys. Chem.*, 1989, **90**, 2154.

14 W. J. Bouma, D. Poppinger and L. Radom, *Isr. J. Chem.*, 1983, **23**, 21.

15 (*a*) D. J. Bellville and N. L. Bauld, *J. Am. Chem. Soc.*, 1982, **104**, 5700; (*b*) S. Lunel and M.-B. Huang, *J. Chem. Soc., Chem. Commun.*, 1989, 1031; (*c*) T. Clark, *J. Am. Chem. Soc.*, 1988, **110**, 1672.

16 A. Ioffe and S. Shaik, *J. Chem. Soc., Perkin Trans. 2*, 1993, 1461.

17 (*a*) R. A. Marcus, *Ann. Rev. Phys. Chem.*, 1964, **15**, 155; (*b*) N. S. Hush, *Trans. Faraday Soc.*, 1961, **57**, 557.

18 Y. Apeloig, O. M. Aharoni, D. Danovich, A. Ioffe and S. Shaik, *Isr. J. Chem.*, 1993, **33**, 387.

19 K. Ohta and K. J. Morokuma, *J. Phys. Chem.*, 1987, **91**, 401.

20 J. S. Littler, *Essays on Free Radical Chemistry*, Special Publ. No. 24, Chemical Society, London, 1973, p. 383.

21 S. Shaik, A. C. Reddy, A. Ioffe, J. P. Dinnocenzo, D. Danovich and J. K. Cho, *J. Am. Chem. Soc.*, 1995, **117**, 3205.

22 A. Pross and S. S. Shaik, *Acc. Chem. Res.*, 1983, **16**, 363.

23 (*a*) S. S. Shaik in *New Concepts for Understanding Organic Reactions*, eds. J. Bertran and G. I. Csizmadia, ASI NATO Series, C267, Kluwer, Dordrecht, 1989, pp. 165–218; (*b*) S. S. Shaik and P. C. Hiberty in *Theoretical Models for Chemical Bonding*, ed. Z. B. Maksic, Springer Verlag, Heidelberg, 1991, Vol. 4; (*c*) A. Pross, *Adv. Phys. Org. Chem.*, 1985, **21**, 99; (*d*) S. S. Shaik, *Prog. Phys. Org. Chem.*, 1985, **15**, 197.

24 S. Shaik, A. Ioffe, A. C. Reddy and A. Pross, *J. Am. Chem. Soc.*, 1994, **116**, 262.

25 L. Eberson and S. S. Shaik, *J. Am. Chem. Soc.*, 1990, **112**, 4489.

26 S. S. Shaik, J. P. Dinnocenzo, *J. Org. Chem.*, 1990, **55**, 3434.

27 R. W. Alder, *J. Chem. Soc., Chem. Commun.*, 1980, 1184.

28 (*a*) X. Ci, R. S. da Silva and D. G. Whitten, *J. Am. Chem. Soc.*, 1989, **111**, 1337; (*b*) X. Ci, R. S. da Silva, J. L. Goodman, D. E. Nicodem and D. G. Whitten, *J. Am. Chem. Soc.*, 1988, **110**, 8548.

29 (*a*) L. Eberson, F. Radner and J. O. Svensson, *J. Chem. Soc., Chem. Commun.*, 1992, 1140; (*b*) L. Eberson and F. Radner, *J. Am. Chem. Soc.*, 1991, **113**, 5825; (*c*) L. Eberson, L. Jönsson, *J. Chem. Soc., Chem. Commun.*, 1980, 1187.

30 C. Amatore, A. Jutand and A. Suarez, *J. Am. Chem. Soc.*, 1993, **115**, 9531.

31 J. P. Dinnocenzo, D. R. Lieberman and T. R. Simpson, *J. Am. Chem. Soc.*, 1993, **115**, 366.

32 G. N. Sastry and S. Shaik, *J. Am. Chem. Soc.*, 1995, **117**, 3290.

33 H. Taube, *Electron Transfer Reactions of Complex Ions in Solution*, Academic Press, New York, 1970.

34 K. F. Purcell and J. C. Kotz, *Inorganic Chemistry*, Saunders, New York, 1977, pp. 659–661.

Paper 4/07757A
Received 20*th December* 1994
Accepted 27*th March* 1995